

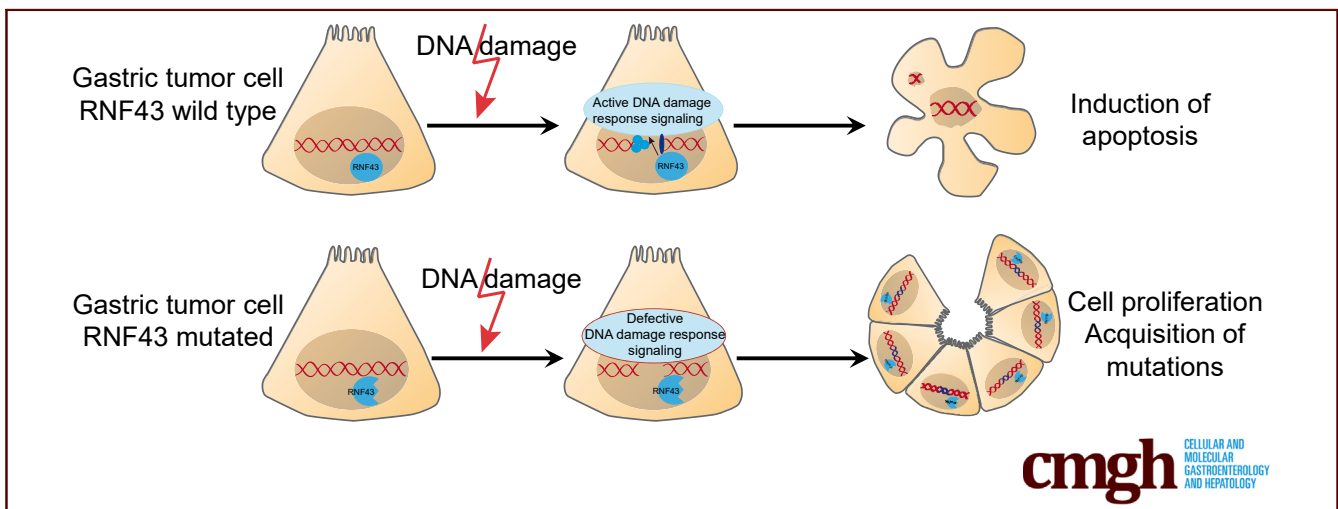
ORIGINAL RESEARCH

Loss of RNF43 Function Contributes to Gastric Carcinogenesis by Impairing DNA Damage Response



Victoria Neumeyer,¹ Anna Brutau-Abia,¹ Michael Allgäuer,¹ Nicole Pfarr,² Wilko Weichert,² Christina Falkeis-Veits,³ Elisabeth Kremmer,⁴ Michael Vieth,³ Markus Gerhard,¹ and Raquel Mejias-Luque¹

¹Institute for Medical Microbiology, Immunology and Hygiene, School of Medicine, Technical University of Munich, Munich, Germany, ²Institute of Pathology, Technical University of Munich, Munich, Germany, ³Institute of Pathology, Klinikum Bayreuth, Bayreuth, Germany, ⁴Institute for Molecular Immunology, Helmholtz Zentrum Munich, German Research Center for Environmental Health (GmbH), Monoclonal Antibody Core Facility, Munich, Germany



SUMMARY

The tumor-suppressor RING finger protein 43 modulates DNA damage response in gastric cells. The RING finger protein 43 mutational status might be used as a biomarker for therapy selection.

BACKGROUND & AIMS: RING finger protein 43 (RNF43) is a tumor suppressor that frequently is mutated in gastric tumors. The link between RNF43 and modulation of Wnt signaling has not been shown clearly in the stomach. Because mutations in *RNF43* are highly enriched in microsatellite-unstable gastric tumors, which show defects in DNA damage response (DDR), we investigated whether RNF43 is involved in DDR in the stomach.

METHODS: DDR activation and cell viability upon γ -radiation was analyzed in gastric cells where expression of RNF43 was depleted. Response to chemotherapeutic agents 5-fluorouracil and cisplatin was analyzed in gastric cancer cell lines and xenograft tumors. In addition, involvement of RNF43 in DDR activation was analyzed upon *Helicobacter pylori* infection in wild-type and *Rnf43* ^{Δ Ex8} mice. Furthermore, a cohort of human gastric biopsy specimens was analyzed for RNF43

expression and mutation status as well as for activation of DDR.

RESULTS: RNF43 depletion conferred resistance to γ -radiation and chemotherapy by dampening the activation of DDR, thereby preventing apoptosis in gastric cells. Upon *Helicobacter pylori* infection, RNF43 loss of function reduced activation of DDR and apoptosis. Furthermore, RNF43 expression correlated with DDR activation in human gastric biopsy specimens, and *RNF43* mutations found in gastric tumors conferred resistance to DNA damage. When exploring the molecular mechanisms behind these findings, a direct interaction between RNF43 and phosphorylated H2A histone family member X (γ H2AX) was observed.

CONCLUSIONS: We identified a novel function for RNF43 in the stomach as a regulator of DDR. Loss of RNF43 function in gastric cells confers resistance to DNA damage-inducing radiotherapy and chemotherapy, suggesting RNF43 as a possible biomarker for therapy selection. (*Cell Mol Gastroenterol Hepatol* 2021;11:1071–1094; <https://doi.org/10.1016/j.jcmgh.2020.11.005>)

Keywords: RNF43; DNA Damage Response (DDR); Gastric Cancer; *Helicobacter pylori*.

Gastric cancer (GC) is the fifth most common malignancy and the third leading cause of cancer-related death worldwide (Global Cancer Observatory (GLOBOCAN) 2018). Several attempts have been made to classify gastric tumors to guide treatment selection.^{1–3} Despite these numerous attempts, surgery is the only curative treatment available to date. Although the addition of chemotherapy or radiotherapy can improve outcomes, prognosis remains poor, with a median survival of 10–12 months and a 5-year survival rate of <10%.⁴ GC patients show a high interindividual as well as intra-individual heterogeneity, making the identification of novel biomarkers indispensable for patient stratification. To date, not many biomarkers for therapy response exist, except for Human epidermal growth factor receptor 2 (HER2) expression or Programmed death-ligand 1 (PD-L1) and microsatellite instability (MSI) levels.^{4–6}

Mutations in well-known tumor suppressors, as well as oncogenes such as *TP53* or *KRAS*, have been identified as drivers of GC.^{3,7,8} Mutations in the E3 ubiquitin ligase RING finger protein 43 (*RNF43*) also have frequently been reported to occur in microsatellite instability (MSI)-high tumors, suggesting an important role of *RNF43* in gastric carcinogenesis.^{3,8–12} Recently, we observed that loss of *RNF43* function enhances the tumorigenic potential of GC cells in vitro and in vivo,¹³ supporting a tumor-suppressor function of *RNF43* in the stomach. The tumor-suppressive function of *RNF43* has been shown to be related to its capacity to negatively regulate Wnt/Wingless-related integration site (WNT) signaling by 2 different mechanisms. Located in the cell membrane, *RNF43* targets Frizzled receptors for ubiquitin-mediated internalization and degradation, thereby decreasing WNT activity.¹⁴ When expressed in the nucleus, we could show that *RNF43* negatively regulates WNT signaling downstream of β -catenin and Adenomatous polyposis coli (APC) by sequestering T-cell factor 4 to the nuclear membrane, thereby suppressing its transcriptional activity.¹⁵ For this inhibitory activity, the presence of an intact RING domain, where the ubiquitin ligase function resides, is essential. Notably, the WNT inhibitory capacity of *RNF43* in the stomach has not been completely demonstrated. Our previous results suggested a WNT-independent function of *RNF43*. Thus, *Rnf43* ^{Δ Ex8} mice carrying an inactivating deletion of the RING domain did not show alterations in the gastric expression of important WNT target genes such as *Axin2* or *Lgr5*. However, we observed thickening of the gastric mucosa, hyperplasia, and cellular atypia in these mice, confirming an important function of *RNF43* in gastric homeostasis.¹³ Nevertheless, the molecular mechanisms involved remained unknown.

Interestingly, ubiquitination of the main players of the DNA damage response (DDR) is a key event for the activation of this signaling cascade, and several E3 ubiquitin ligases have been reported to be involved.^{16–19} The DDR is critical for maintaining genomic stability commonly lost in tumors. Two main kinase-signaling pathways, ataxia-telangiectasia mutated (ATM)–checkpoint kinase 2 (CHK2) and ATM- and Rad3-Related (ATR)–CHK1, coordinate cellular

responses to DNA damage. ATM–CHK2 signaling is activated by radiation and genotoxins inducing double-strand breaks (DSBs), while ATR–CHK1 is activated when replication is impeded.²⁰ Mutations in ATR or CHK1 were found in gastric tumors with MSI,²¹ and mutated ATM was associated strongly with MSI,²² indicating that inhibition of DDR might be important for the development of gastric tumors harboring MSI.

Helicobacter pylori infection, one of the major risk factors for the development of GC, has been linked to DDR. *H. pylori* elicits an immune response that leads to the production of reactive oxygen and nitrogen species, which can induce DNA damage.^{23,24} In addition, *H. pylori* has been shown to induce DSBs directly in host cells.^{25,26} Furthermore, *H. pylori* infection induces epigenetic modifications leading to the up-regulation of ATM.²⁷ Thus, induction of DNA damage by infection and lack of functional repair mechanisms can highly contribute to gastric carcinogenesis.

Considering the high mutation rate of *RNF43* in gastric tumors showing MSI and our previous data showing that in vivo loss of *RNF43* function leads to gastric pathology independent of alterations in WNT signaling,¹³ we sought to determine whether *RNF43* could be involved in DDR in the stomach and thereby influence response to DNA damage-inducing cancer therapy.


Results

Loss of *RNF43* Function Confers Resistance to DNA Damage-Induced Cell Death

To explore whether *RNF43* is involved in DDR, we first analyzed the levels of phosphorylated H2A histone family member X (γ H2AX) and CHK2 in AGS control and in AGS cells where expression of *RNF43* had been depleted by CRISPR/Cas9 (*AGS*^{deletion at aspartic acid 196 [D196]fs}) (Figure 1A). Cellular damage caused by γ -radiation highly induced H2AX and CHK2 phosphorylation in cells expressing *RNF43* (Figure 1B). Depletion of *RNF43* expression resulted in reduced activation of DDR because lower levels of γ H2AX and phosphorylated CHK2 were detected in *AGS*^{D196fs} cells (Figure 1B).

No single clones could be obtained for MKN45 cells after transfection of the guide RNAs. Therefore, we depleted *RNF43* by lentiviral transduction of specific short hairpin

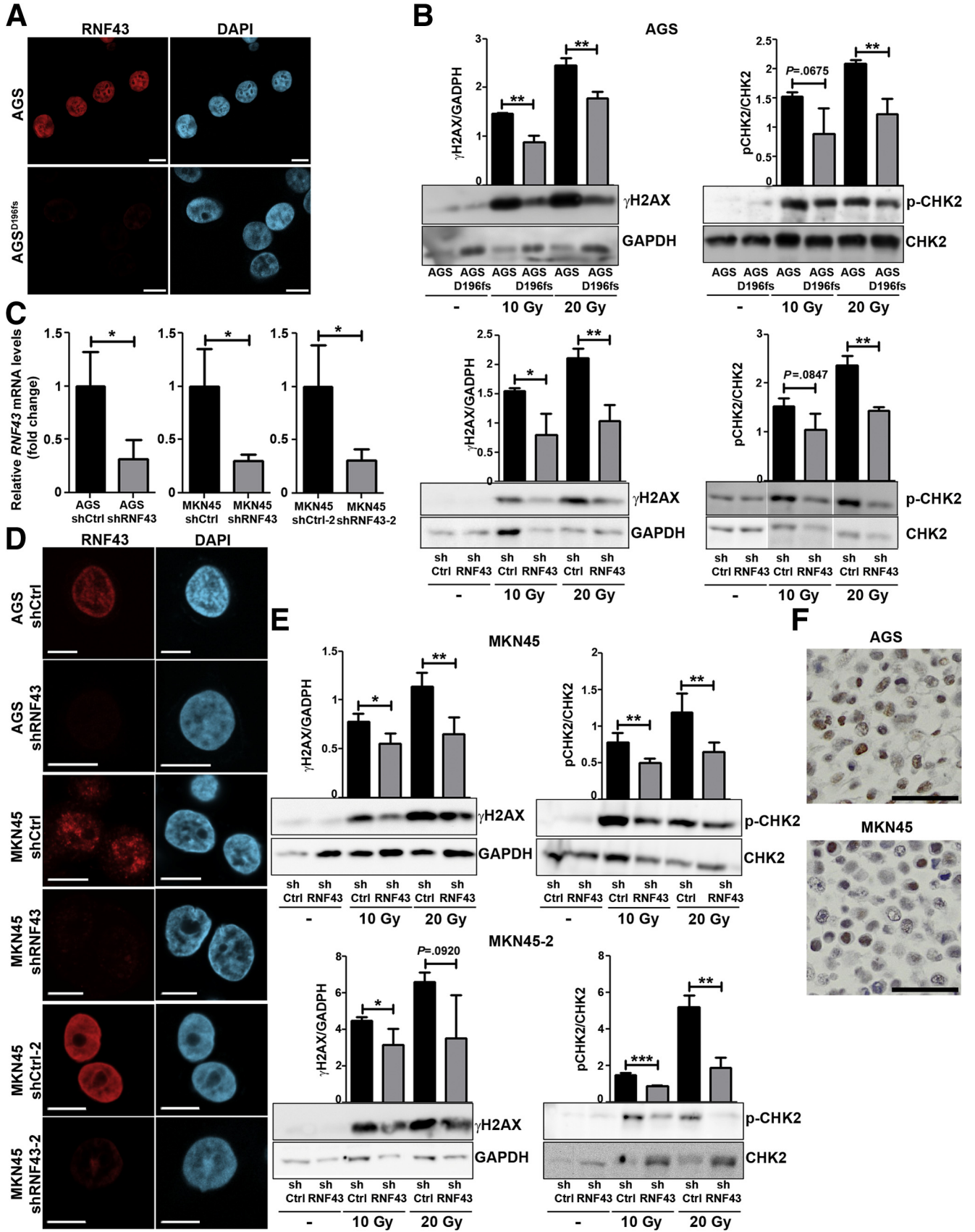
Abbreviations used in this paper: ATM, ataxia-telangiectasia mutated; ATR, ATM- and Rad3-Related; CHK, checkpoint kinase; CRISPR/Cas9, Clustered related interspaced short palindromic repeats/CRISPR associated 9; D196, deletion at aspartic acid 196; DDR, DNA damage response; DSB, double-strand break; GC, gastric cancer; H2AX, H2A histone family member X; MSI, microsatellite unstable; MSI-high, microsatellite instability-high; PMSS1, pre-mouse SS1; RNF43, RING finger protein 43; RNP, ribonucleoprotein; SDS, sodium dodecyl sulfate; shControl, short hairpin control; shRNF43, short hairpin RING finger protein 43; SNP, single-nucleotide polymorphism; WNT, Wingless-related integration site; WT, wild-type.

 Most current article

© 2021 The Authors. Published by Elsevier Inc. on behalf of the AGA Institute. This is an open access article under the CC BY-NC-ND license (<http://creativecommons.org/licenses/by-nc-nd/4.0/>).

2352-345X

<https://doi.org/10.1016/j.jcmgh.2020.11.005>



RNAs (Figure 1C and D). Similar to our observations in AGS^{D196fs} cells, impaired activation of DDR was observed in MKN45–short hairpin RNF43 (shRNF43) and AGS–shRNF43 cells (Figure 1E and B, respectively). These observations indicate that RNF43 is important for the induction of DDR in gastric cells.

It has to be noted that AGS and MKN45 cells do not show mutations in *RNF43* (Catalogue Of Somatic Mutations In Cancer (Cosmic) ID: COSS906790 and COSS925340, respectively), and therefore express wild-type (WT) protein in the nucleus (Figure 1F).

Interestingly, increased levels of *RNF43* messenger RNA were detected in AGS and MKN45 GC cells after applying different doses of γ -radiation (Figure 2A), suggesting that DNA damage induces the expression of RNF43.

We next measured cell viability upon induction of DNA damage through γ -radiation. AGS^{D196fs} cells showed enhanced cell viability after irradiation (Figure 2B). RNF43 knock-down MKN45 and RNF43 knock-down AGS cells showed increased cell viability compared with short hairpin control (shControl)-transduced cells upon treatment with ionizing radiation (Figure 2B). Notably, depletion of *RNF43* either by Clustered related interspaced short palindromic repeats (CRISPR)/ CRISPR associated 9 (Cas9) or short hairpin RNAs already induced changes in cell proliferation under basal conditions (Figure 2C), which were accounted for when comparing cell viability of WT and *RNF43*-depleted cells after γ -radiation.

Cell survival after radiation also was assessed in clonogenic assays. Loss of RNF43 enhanced clonal proliferative capacity of gastric cells because more colonies of AGS^{D196fs} and MKN45–shRNF43 compared with respective controls were detected after exposing the cells to γ -radiation (Figure 2D).

Activation of DDR results in cellular apoptosis when the repair mechanisms cannot cope with the cellular damage inflicted. Thus, we next evaluated whether enhanced viability of cells lacking RNF43 expression upon γ -radiation was the result of reduced cellular apoptosis. We observed that a higher percentage of AGS- and MKN45-expressing WT RNF43 underwent early (Annexin V-positive) and late apoptosis (Annexin V/propidium iodide-double-positive) compared with AGS^{D196fs} and MKN45–shRNF43 cells (Figure 2E).

Together, our results indicate that RNF43 is involved in DDR in GC cells and depletion of its expression confers resistance to DNA damage-induced apoptosis.

RNF43 Influences Susceptibility to DNA Damage-Inducing Chemotherapeutics

Current GC therapeutic treatments are based on the use of DNA damage-inducing chemotherapeutics, such as cisplatin or 5-fluorouracil.²⁸ To analyze whether depletion of RNF43 influenced the response of GC cells to DNA damage-inducing chemotherapeutics, we analyzed cell viability in AGS control and AGS^{D196fs} cells upon treatment with lethal doses 50 (LD50) of 5-fluorouracil and cisplatin. AGS^{D196fs} showed higher cell viability after treatment when compared with control cells (Figure 3A), indicating that depletion of RNF43 confers resistance to chemotherapy. Similar results were observed for MKN45–shRNF43 and AGS–shRNF43 cells (Figure 3A).

The expression of *RNF43* was increased in AGS and MKN45 cells treated with 5-fluorouracil and cisplatin (Figure 3B), confirming up-regulation of RNF43 in response to DNA damage.

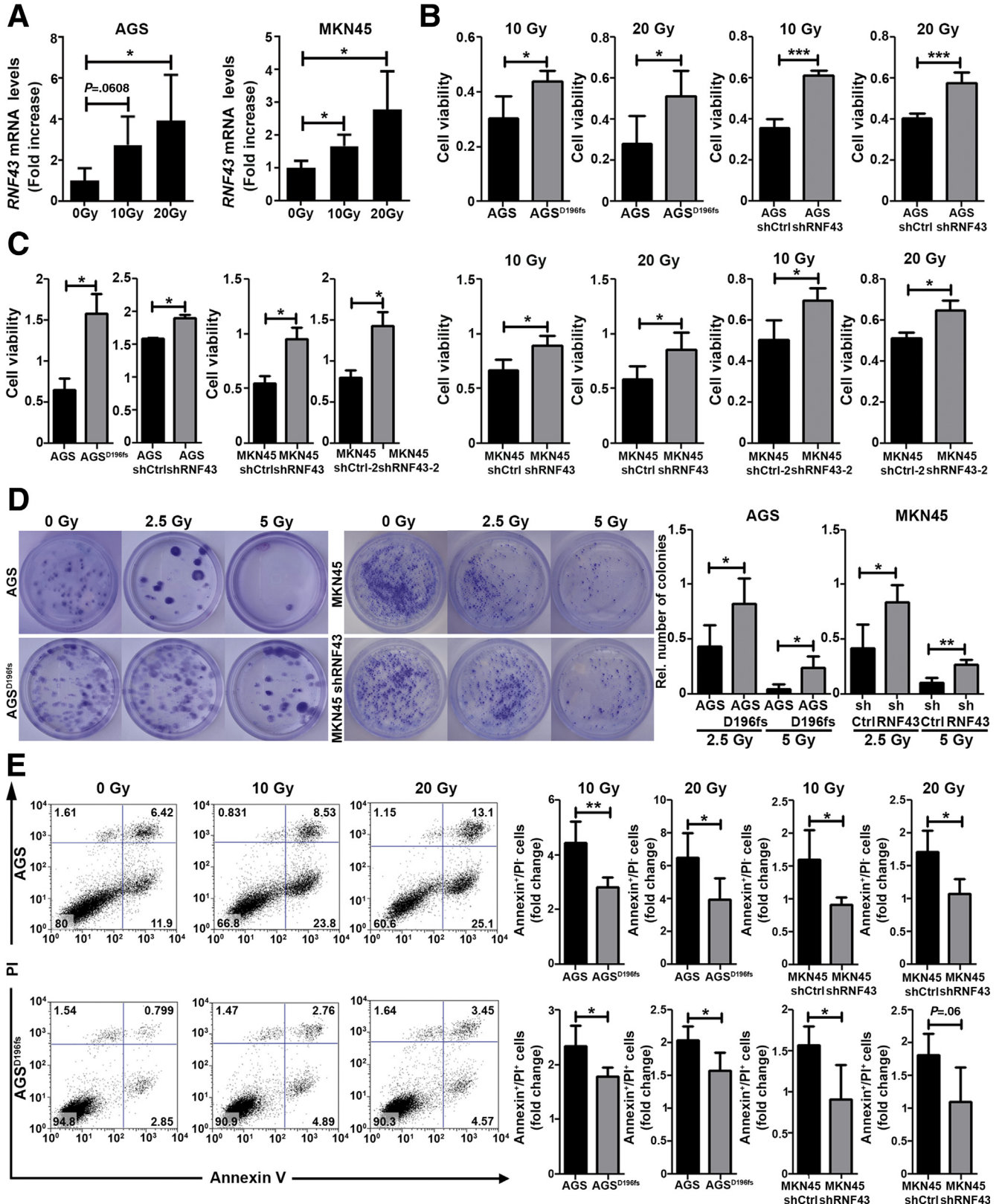
Resistance to chemotherapy after depletion of RNF43 expression was explored further in a tumor xenograft model. When tumors originating from MKN45–shControl and MKN45–shRNF43 cells reached 40–70 mm³, mice were treated with 5-fluorouracil or cisplatin. Tumors derived from MKN45–shRNF43 cells grew bigger compared with tumors that originated from MKN45–shControl cells, as previously reported.¹³ Therefore, tumor growth upon treatment with chemotherapeutics was calculated relative to the initial tumor size to account for the growth-promoting effect of RNF43 loss. Tumors derived from MKN45–shRNF43 cells showed enhanced resistance to chemotherapy in vivo because bigger tumors were observed after treatment (Figure 3C and D), confirming the results observed in vitro. In addition, we evaluated activation of the DDR, apoptosis, and proliferation by staining the tumors for γ H2AX, cleaved-caspase 3, and Ki67, respectively, at the end point of treatment with 5-fluorouracil (Figure 4A) or cisplatin (Figure 4B). Tumors derived from MKN45–shRNF43 cells showed reduced levels of γ H2AX upon treatment with 5-fluorouracil, indicating lower activation of DDR (Figure 4A). Furthermore, reduced apoptosis and increased proliferation were observed in MKN45–shRNF43-derived tumors (Figure 4A) compared with tumors that originated from MKN45–shControl cells. Likewise, after treatment with cisplatin, tumors derived from MKN45–shRNF43 cells showed reduced DDR activation and apoptosis (Figure 4B). These tumors also were more proliferative compared with tumors originating from MKN45–shControl cells (Figure 4B). Together, these results

Figure 1. (See previous page). **RNF43 is involved in DDR.** (A) Representative immunofluorescence images of RNF43 (red) in control and AGS^{D196fs} cells. Scale bars: 10 μ m. (B) Western blot analysis and quantification of γ H2AX and CHK2 expression in WT AGS, AGS^{D196fs}, control AGS (shCtrl), and RNF43 knockdown AGS (shRNF43) cells after γ -radiation. GAPDH was used as a protein loading control (N = 3). (C) *RNF43* mRNA levels in control and RNF43 knockdown AGS and MKN45 cells. Cycle threshold (C_T) values were normalized to *GAPDH* and fold change was calculated over control cells. (D) Representative immunofluorescence images of RNF43 (red) in control and RNF43 knockdown AGS and MKN45 cells. Scale bars: 10 μ m. (E) Western blot analysis and quantification of γ H2AX and CHK2 expression in control MKN45 (shCtrl) and RNF43 knockdown MKN45 (shRNF43) cells after γ -radiation. GAPDH was used as a protein loading control (N = 3). (F) Endogenous RNF43 expression in AGS and MKN45 cells detected by immunocytochemistry. Scale bar: 50 μ m. Error bars indicate SD. **P* \leq .05, ***P* \leq .01, ****P* \leq .001, 2-tailed unpaired *t* test. DAPI, 4',6-diamidino-2-phenylindole; GAPDH, glyceraldehyde-3-phosphate dehydrogenase; mRNA, messenger RNA.

suggest that, in the absence of RNF43, GC cells become resistant to chemotherapeutics.

To further substantiate resistance to DNA damage-inducing chemotherapeutics after loss of RNF43 function,

we generated gastric organoids from WT and *Rnf43*^{ΔEx8} mice.¹³ Organoids were treated with 5-fluorouracil or cisplatin, and cell viability was measured after 4 days. Organoids derived from *Rnf43*^{ΔEx8} mice were more resistant



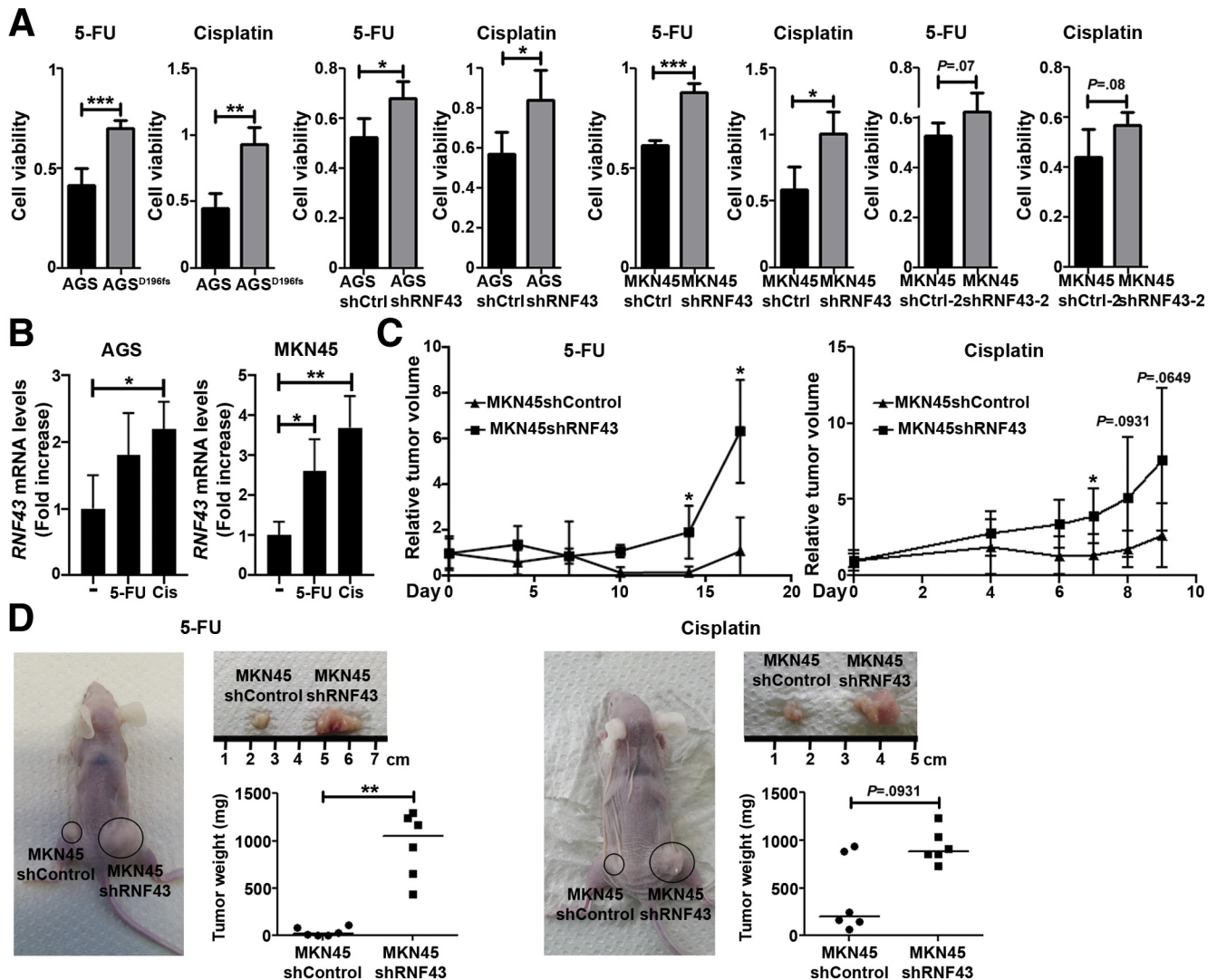


Figure 3. RNF43 influences susceptibility to DNA damage-inducing chemotherapeutics. (A) Cell viability of WT AGS, AGS^{D196fs}, control MKN45 and AGS (shCtrl), and RNF43 knockdown MKN45 and AGS (shRNF43) cells after treatment with 5-fluorouracil (5-FU) or cisplatin. Values were normalized over untreated cells (N = 3). (B) RNF43 mRNA levels in AGS and MKN45 GC cells after treatment with 5-FU or cisplatin (Cis) for 48 hours. Cycle threshold (C_T) values were normalized to GAPDH and fold change was calculated over untreated cells (N = 3). (C) Relative volume of xenograft tumors derived from control MKN45 (shCtrl) and RNF43 knockdown MKN45 (shRNF43) cells after treatment of mice with 5-FU or cisplatin. Relative volumes were calculated over tumor volume before treatment (N = 6/group). (D) Representative images of xenograft tumors derived from control MKN45 (shCtrl) and RNF43 knockdown MKN45 (shRNF43) cells after treatment of mice with 5-FU or cisplatin. Size and weight of the resected tumors are shown (n = 6/group). Error bars indicate SD. Horizontal lines represent the median values. *P ≤ .05, **P ≤ .01, and ***P ≤ .001, (A and B) 2-tailed unpaired t test, (C and D) Mann–Whitney test.

to treatment with chemotherapeutics inflicting DNA damage (Figure 4C), confirming the results observed in vitro and in the xenograft model.

Finally, we assessed whether levels of RNF43 correlate with response to chemotherapy using human gastric organoids. Organoids were generated from stomach biopsy specimens

Figure 2. (See previous page). Loss of RNF43 function confers resistance to DNA damage-induced cell death. (A) RNF43 mRNA levels in AGS and MKN45 gastric cancer cells upon increasing doses of γ -radiation. Cycle threshold (C_T) values were normalized to GAPDH and fold change was calculated over untreated cells (N = 4). (B) Cell viability of WT AGS, AGS^{D196fs}, control MKN45 (shCtrl), and RNF43 knockdown MKN45 (shRNF43) cells after γ -radiation. Values were normalized over untreated cells (N = 4). (C) Cell viability of AGS, AGS^{D196fs} cells, as well as control AGS and MKN45 (shCtrl) and RNF43 knockdown AGS and MKN45 (shRNF43) cells under basal conditions (N = 3). (D) Representative images and quantification of cell colonies after γ -radiation (N = 4). (E) Flow cytometry analysis of Annexin V and propidium iodide (PI)-positive AGS and MKN45 cells after irradiation. Values were normalized over untreated cells (N = 4). Error bars indicate SD. *P ≤ .05, **P ≤ .01, ***P ≤ .001, 2-tailed unpaired t test. mRNA, messenger RNA.

and treated with 5-fluorouracil or cisplatin for 5 days, after which cell viability was measured. An inverse correlation between response to 5-fluorouracil treatment and RNF43 expression was observed (Spearman $r_s = -0.6264$; $P = .0220$) (Figure 4D). RNF43 expression was higher in organoids responding to 5-fluorouracil than in organoids not responding (Figure 4D). Similar results were detected when human gastric organoids were treated with cisplatin (Figure 4E).

These results suggest that cells lacking RNF43 function become resistant to DNA damage-inducing chemotherapeutics.

Because RNF43 has been described to inhibit WNT signaling in different cellular models, we analyzed whether the effects induced by depleting RNF43 expression depended on alterations in WNT. We assessed the expression levels of the WNT target genes *AXIN2* and *LGR5* in AGS control and AGS^{D196fs} and MKN45-shControl and MKN45-shRNF43. No differences in the expression of these genes were detected (Figure 4F), indicating that the effects are independent of changes in WNT signaling.

RNF43 Is Involved in *H. pylori*-Induced DNA Damage Response

H. pylori has been described to induce DNA damage in gastric epithelial cells.²⁵ We analyzed whether activation of DDR in response to *H. pylori* infection is compromised in cells with suppressed *RNF43* expression. Indeed, we observed that activation of DDR, as assessed by H2AX and CHK2 phosphorylation, was reduced in AGS^{D196fs} cells (Figure 5A), indicating that RNF43 is involved in DDR elicited by *H. pylori*. Likewise, impairment of DDR in response to *H. pylori* infection was detected in MKN45-shRNF43 and AGS-shRNF43 cells (Figure 5A).

H. pylori infection up-regulated the expression of *RNF43* in AGS and MKN45 cells (Figure 5B). In addition, we observed that the expression of *RNF43* was higher in gastric biopsy specimens from *H. pylori*-infected patients compared with noninfected individuals (Figure 5C).

To further explore the involvement of RNF43 in DDR upon *H. pylori* infection in vivo, we infected WT or *Rnf43*^{ΔEx8} mice with the *H. pylori* pre-mouse SS1 (PMSS1) strain and killed them after 3 months. As previously reported, at this age, *Rnf43*^{ΔEx8} mice did not show pathologic changes in the stomach.¹³ *H. pylori* infection up-regulated the expression of *Rnf43* in the stomach of WT mice (Figure 5D). Notably, *Rnf43*^{ΔEx8} mice were colonized at lower levels than WT mice (Figure 6A) and showed more severe gastric inflammation (Figure 6A). Increased recruitment of CD3⁺ cells into the stomach was observed in *Rnf43*^{ΔEx8} mice when compared with WT infected mice (Figure 6A). In addition, increased infiltration of neutrophils and mast cells was detected in *Rnf43*^{ΔEx8} mice (Figure 6A). Concomitantly, *Rnf43*^{ΔEx8} mice showed increased expression levels of the proinflammatory cytokines *Cxcl1* (murine homologue of interleukin 8), *Ifng*, and *Tnfa* (Figure 6B).

We next assessed activation of DDR response upon *H. pylori* infection by analyzing γ H2AX-positive cells in the

stomach of WT and *Rnf43*^{ΔEx8} mice. *H. pylori* infection resulted in increased levels of γ H2AX-positive cells in WT mice. In contrast, no increase in the induction of DDR was detected in infected *Rnf43*^{ΔEx8} mice, which showed lower numbers of γ H2AX-positive cells when compared with infected WT mice (Figure 6A). In addition, *Rnf43*^{ΔEx8} mice showed reduced apoptosis compared with WT mice, as shown by fewer cleaved caspase 3-positive cells in the stomach after infection (Figure 6A).

We also analyzed whether the changes observed in *Rnf43*^{ΔEx8} mice could be related to WNT activation by staining stomach tissue samples of naïve and infected mice for β -catenin. β -catenin expression was up-regulated upon infection in WT as well as in *Rnf43* mutant mice, confirming activation of WNT signaling by *H. pylori*. However, no differences between wild-type and *Rnf43*^{ΔEx8} mice were observed (Figure 6A).

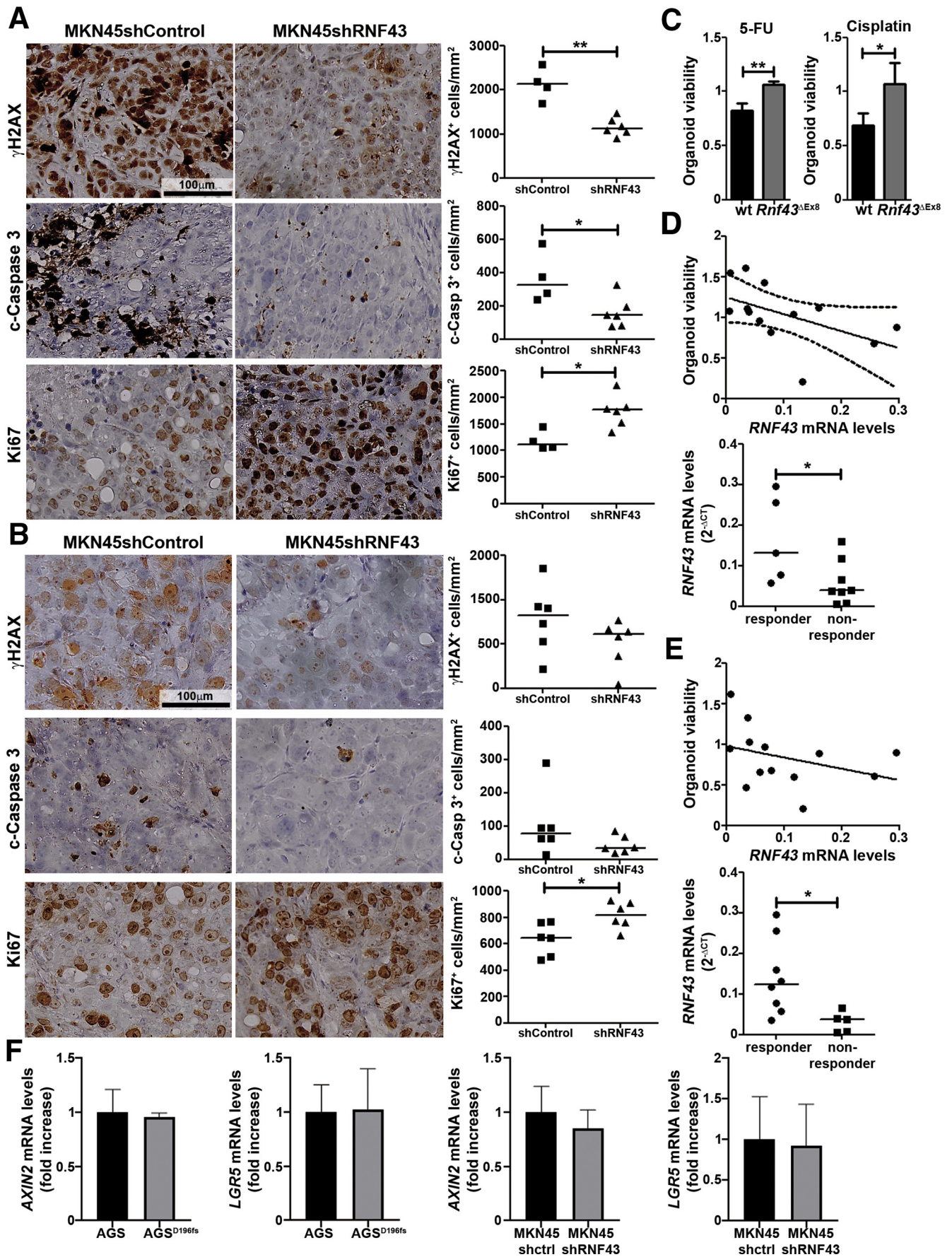
Together, these results indicate that loss of *Rnf43* aggravates *H. pylori*-induced inflammation, but at the same time results in reduced DDR. In addition, these effects are independent of alterations in the WNT pathway.

RNF43 Expression Varies During Gastric Carcinogenesis

Our results indicate that *H. pylori* infection induces RNF43 expression, which relates to induction of DDR. To further confirm these observations in human tissue, we analyzed human gastric biopsy specimens from healthy, as well as *H. pylori*-infected subjects presenting with gastritis (Table 1). A higher number of RNF43 and γ H2AX-positive cells was detected in *H. pylori*-positive gastritis compared with healthy mucosa (Figure 7A), confirming that *H. pylori* infection up-regulates RNF43 expression and induces DNA damage in gastric cells. We further analyzed intestinal metaplasia and gastric tumor samples (Table 1), the latter restricted to intestinal- and diffuse-type tumors according to Lauren's¹ classification. Increased expression of RNF43 was observed in all gastric lesions analyzed (Figure 7A). Interestingly, expression of RNF43 correlated to γ H2AX levels in intestinal metaplasia (Spearman $r_s = 0.7103$; $P < .0001$) as well as in diffuse-type gastric tumors (Spearman $r_s = 0.4426$; $P = .0267$) (Figure 7B), although no correlation could be observed in gastritis or intestinal-type gastric tumors (Figure 7B).

RNF43 Mutations Upstream of the RING Domain Confer Resistance to DNA Damage

RNF43 was observed to be mutated frequently in gastric tumors. To determine whether our samples carried WT or mutated *RNF43*, we sequenced a subset of intestinal metaplasia ($n = 12$), intestinal-type ($n = 15$), and diffuse-type ($n = 13$) gastric tumors. No mutations in *RNF43* were detected in intestinal metaplasia samples. Three of the 12 samples analyzed harbored mutations in *APC* (p.A1471Gfs*14; p.R1463fs; p.R1450X). In 2 cases, *APC* mutation co-occurred with a mutation in *BRAF* (p.N581S) and *KRAS* (p.G13D), respectively. Mutated *ERBB4* (p.L713V) was observed in 1 of the intestinal metaplasia cases (Table 2).



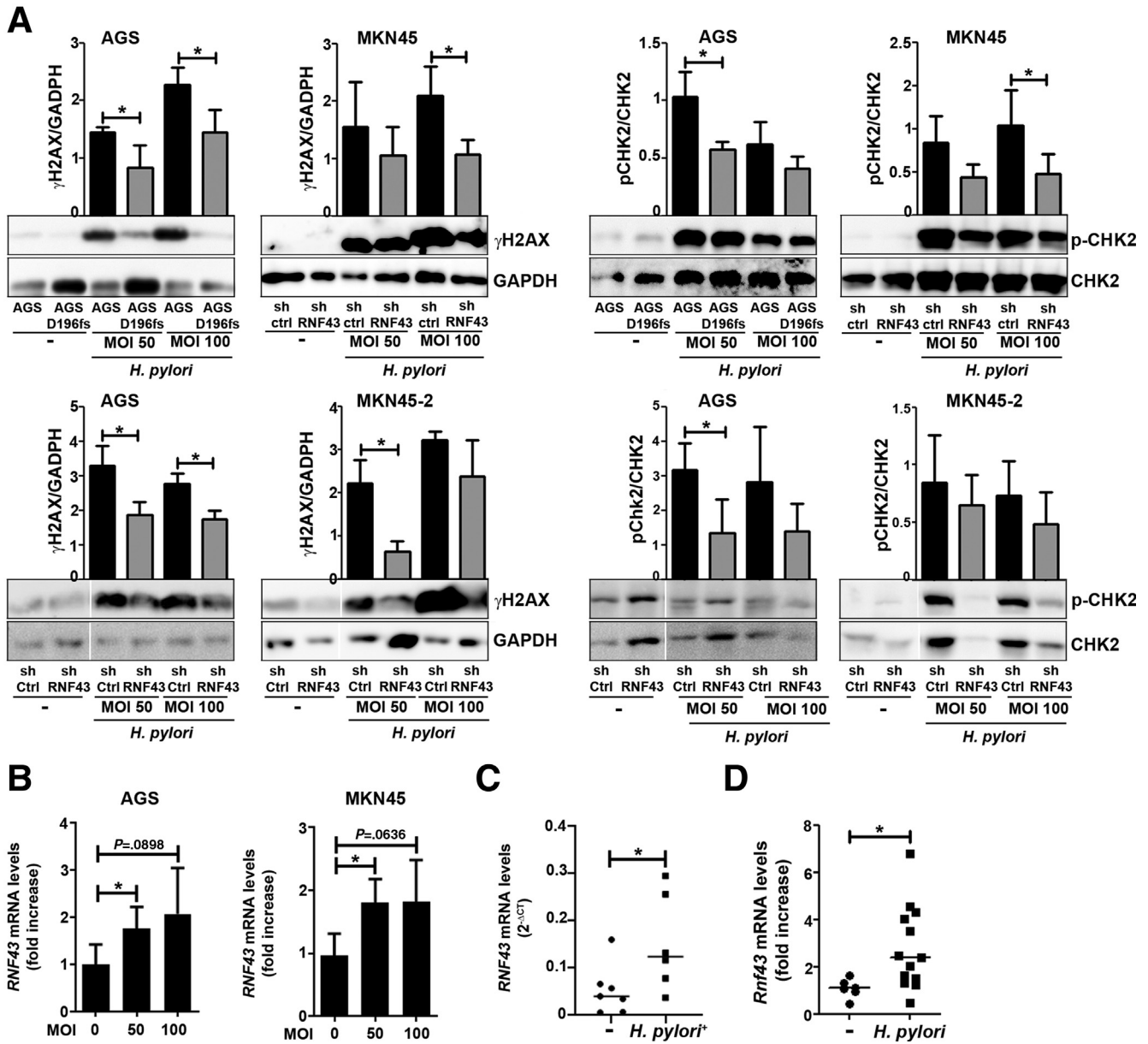
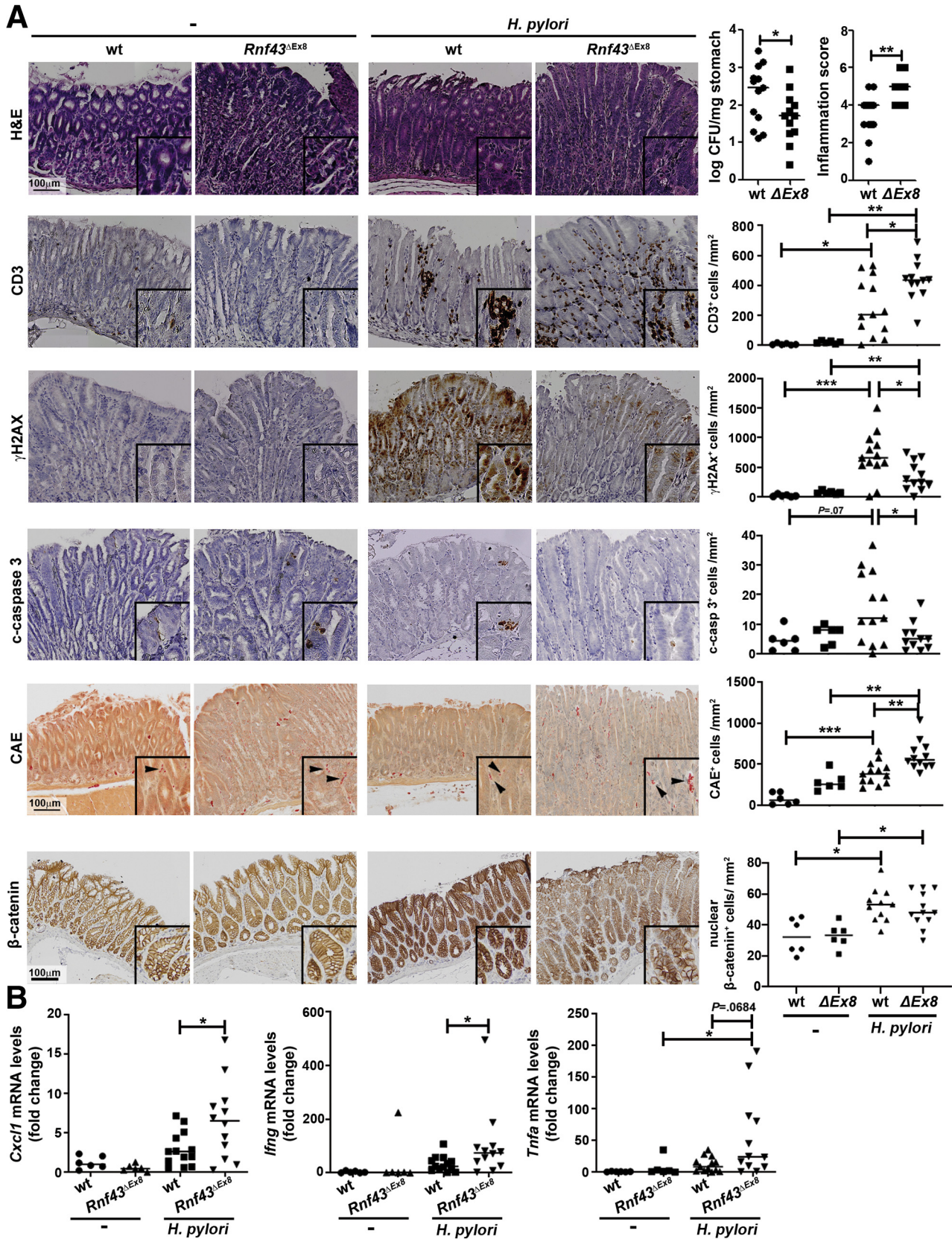


Figure 5. RNF43 is involved in *H. pylori*-induced DDR. (A) Western blot analysis and quantification of γ H2AX and CHK2 expression in WT AGS, AGS^{D196fs}, control MKN45 and AGS (shCtrl), and RNF43 knockdown MKN45 and AGS (shRNF43) cells upon *H. pylori* PMSS1 infection at different multiplicity of infection (MOI). GAPDH was used as a loading control (N = 4). (B) *RNF43* mRNA levels after *H. pylori* infection of AGS and MKN45 cells. Cycle threshold (C_T) values were normalized to GAPDH and fold change was calculated over uninfected cells (N = 4). (C) *RNF43* mRNA levels normalized to GAPDH in gastric biopsy specimens from uninfected (n = 6) and *H. pylori*-infected (n = 6) subjects. (D) *Rnf43* mRNA levels in the stomach of WT mice (n = 13) after 3-month *H. pylori* PMSS1 infection. C_T values were normalized to *Gapdh* and fold change was calculated over uninfected mice (n = 6). Error bars indicate SD. *P ≤ .05, (A and B) 2-tailed unpaired t test, (C and D) Mann-Whitney test. GAPDH, glyceraldehyde-3-phosphate dehydrogenase; mRNA, messenger RNA.

Figure 4. (See previous page). RNF43 influences susceptibility to DNA damage-inducing chemotherapeutics. Representative images showing γ H2AX, cleaved caspase 3 (c-caspase 3), and Ki67 detected by immunohistochemistry in xenograft tumors that originated from control MKN45 (shCtrl) and RNF43 knockdown MKN45 (shRNF43) cells after treatment with (A) 5-fluorouracil or (B) cisplatin. Quantification of positive cells per square millimeter is shown. Each dot represents 1 mouse. (C) Viability of gastric organoids from WT or *Rnf43*^{ΔEx8} mice after treatment with 5-fluorouracil (5-FU) or cisplatin. Values were normalized over untreated (N = 3). Spearman correlation between *RNF43* mRNA expression levels in human gastric tissue samples (N = 13), and viability of organoids generated from the same tissue samples after treatment with (D) 5-fluorouracil or (E) cisplatin. *RNF43* mRNA levels normalized to GAPDH also are shown. (F) *AXIN2* and *LGR5* mRNA levels in AGS, AGS^{D196fs}, and MKN45 control and RNF43 knockdown cells. Cycle threshold (C_T) values were normalized to GAPDH and fold change was calculated over control cells (N = 3). Error bars indicate SD. Horizontal lines represent the median values. *P ≤ .05, **P ≤ .01, (C and F) 2-tailed unpaired t test, (A, B, D, and E) Mann-Whitney test. mRNA, messenger RNA.

Mutations in *RNF43* were found only in gastric tumors. Two of the intestinal-type gastric tumors carried mutated *RNF43* (p.D628G and p.R371R; p.R132X). Interestingly, 5 of

the 15 cases analyzed presented mutations in *TP53*. *RNF43* was mutated in 2 diffuse-type tumors (p.R584fs; p.R132X). In this subset of tumors, mutations in *CDH1* were the most



frequent (4 of 13 cases), as expected for this type of stomach cancer. A summary of the mutations can be found in Table 2. RNF43 mutations have been found more frequently in MSI-high tumors. Mutated diffuse-type tumors were genomically stable, as expected.³ In contrast, 1 of the intestinal-type tumors carrying mutated RNF43 was MSI-high (Table 2).

In most of the cases analyzed we found single-nucleotide polymorphism (SNP) variants of *RNF43*, namely I47V (rs3744093), R117H (rs2257205), L418M (rs2526374), and P686R (rs9652855) (Table 2). It recently was shown that a SNP of the *RNF43* X117 site is associated with overall survival of colorectal cancer patients.²⁹ To determine whether this could be related to an altered response to DNA damage-inducing chemotherapy, we sequenced human gastric organoids to identify SNPs and analyzed their response to 5-fluorouracil and cisplatin. Five SNPs were found frequently. The I47V variant was found in 23 of the 40 cases (57.5%). Nine cases carried the R117H variant (22.5%). The L418M variant was observed in 18 cases (45%), and the P686R variant was observed in 7 cases (17.5%). In 6 cases (15%) we found the variant R343H (rs34523089), which was detected in only 2 tumor samples (Table 2). No difference in response to chemotherapy was detected between samples harboring WT *RNF43* and samples presenting any of the aforementioned SNPs (Figure 8A).

To determine whether the mutations occurring in tumors conferred resistance to γ -radiation, we selected 2 mutations observed in our tumor cohort and generated AGS cells carrying these mutations by CRISPR/CAS9 editing. We selected mutations occurring before (p.R132X) or downstream of the RING domain (p.R584fs). After transfection of guide RNAs we could not introduce the indicated mutations but obtained cells carrying the frameshift mutations A136fs and Q577fs, respectively. Because these mutations give rise to similar proteins, we used the generated AGS^{A136fs} and AGS^{Q577fs} in further experiments. AGS^{A136fs} cells showed resistance to γ -radiation as more colonies were observed (Figure 8B). In contrast, AGS^{Q577fs} cells were as sensitive to γ -radiation as WT cells. Similarly, the frameshift mutation A136fs conferred increased resistance to chemotherapy in AGS cells (Figure 8C), while the viability of cells expressing the Q577fs mutation after 5-fluorouracil or cisplatin treatment was similar to the viability of AGS WT cells.

These findings show that mutations upstream of the RING domain of RNF43 in gastric cells confer resistance to DNA damage-inducing agents, and confirm the importance of the RING domain for proper function of the protein.

RNF43 Regulates DNA Damage Response by Ubiquitinating γ H2AX

We finally explored the molecular mechanism by which RNF43 regulates DDR. We observed that upon induction of DNA damage, RNF43 co-localized with γ H2AX in the nucleus of irradiated cells (Figure 9A and B). Moreover, direct interaction between RNF43 and γ H2AX was detected in co-immunoprecipitation experiments after irradiation of AGS cells (Figure 9C).

We next analyzed whether RNF43 influenced γ H2AX ubiquitination status. To this end, we immunoprecipitated γ H2AX in AGS^{D196fs} and MKN45shRNF43 cells and detected K48 and K63 ubiquitination by Western blot. We observed that ubiquitination of γ H2AX was reduced in RNF43-depleted cells (Figure 9D), indicating that RNF43 is involved in DDR by interacting and ubiquitinating γ H2AX.

Discussion

Several studies have shown that *RNF43* is mutated in tumors of the gastrointestinal tract, including colorectal, pancreatic, and GC. *RNF43* mutations found in GC were considered driving mutations of gastric carcinogenesis,⁸ occurring early during transition of adenomas to carcinomas.³⁰ Functionally, the importance of RNF43 for tissue homeostasis derives from its role as an inhibitor of the WNT signaling pathway.^{14,15} However, our previous data suggest that the tumor-suppressor activity of RNF43 in gastric cells is independent of WNT. In a xenograft model using human gastric epithelial cells with lentiviral-mediated silencing of RNF43, we observed no changes in the activation of WNT signaling. In addition, gastric alterations detected in *Rnf43* ^{Δ Ex8} mice were not related to changes in the expression of WNT target genes,¹³ indicating that RNF43 might have an alternative function in the stomach. Interestingly, various RING finger proteins have been reported to play important roles in DDR by ubiquitinating the central histone H2AX. For instance, a complex of RNF2 and RNF51 ubiquitinates γ H2AX at the lysine residues K118/K119,³¹ while RNF8 and RNF168 attach further K63-linked ubiquitin chains to this histone.^{17,18,32} RNF168 also has been described to ubiquitinate γ H2AX at the lysine residues K13/K15, which has been shown to be important for DDR signaling.³³ In our study, we observed that loss of RNF43 function resulted in reduced levels of K63- and K48-linked γ H2AX ubiquitination upon irradiation, which translated into impaired DDR activation and enhanced cellular survival. These results indicate an important role of RNF43 in DDR because ubiquitination of γ H2AX has been described

Figure 6. (See previous page). RNF43 is involved in *H pylori*-induced DDR. (A) Colony forming units (CFU)/mg of stomach of WT (n = 13) and *Rnf43* ^{Δ Ex8} mice (n = 12), and inflammatory score after *H pylori* infection. Activity and chronicity were evaluated in antrum and corpus according to the updated Sydney system. Representative images and quantification of CD3, γ H2AX, cleaved-caspase 3 (c-casp3), chloroacetate esterase (CAE)-positive cells (neutrophils and mast cells), and nuclear β -catenin-positive cells per square millimeter of tissue stained by immunohistochemistry in murine gastric tissue samples are shown. Arrowheads indicate positive cells. (B) *Cxcl1*, *Ifn γ* , and *Tnfa* mRNA levels in the stomach after 3-month *H pylori* PMSS1 infection. Cycle threshold (C_T) values were normalized to *Gapdh* and fold change was calculated over uninfected mice. Horizontal lines represent the median values. *P \leq .05, **P \leq .01, and ***P \leq .001, Mann-Whitney test. mRNA, messenger RNA.

Table 1. List of Human Gastric Biopsy Specimens Classified by Gastric Pathology Observed

Sample ID	Sex	Age, y	<i>H pylori</i> status
Healthy stomach			
H1	M	76	Negative
H2	M	55	Negative
H3	F	90	Negative
H4	F	80	Negative
H5	F	39	Negative
H6	M	72	Negative
H7	F	84	Negative
H8	M	59	Negative
H9	M	69	Negative
H10	M	27	Negative
H11	F	62	Negative
H12	M	59	Negative
H13	M	72	Negative
H14	M	33	Negative
H15	F	50	Negative
H16	F	24	Negative
H17	F	27	Negative
H18	F	41	Negative
H19	F	22	Negative
H20	F	27	Negative
Gastritis			
G1	M	60	Positive
G2	M	57	Positive
G3	M	59	Positive
G4	F	60	Positive
G5	F	32	Positive
G6	M	58	Positive
G7	F	85	Positive
G8	F	73	Positive
G9	M	90	Positive
G10	F	83	Positive
G11	F	72	Positive
G12	F	78	Positive
G13	F	82	Positive
G14	M	60	Positive
G15	M	90	Positive
G16	M	91	Positive
G17	M	47	Positive
G18	F	48	Positive
G19	F	32	Positive
G20	M	74	Positive
G21	F	81	Positive
G22	F	52	Positive
G23	M	90	Positive
G24	M	68	Positive
Intestinal metaplasia			
IM1	M	76	Eradicated
IM2	M	81	Negative
IM3	F	67	Eradicated
IM4	F	80	Negative
IM5	F	68	Eradicated
IM6	M	55	Eradicated
IM7	M	31	Eradicated
IM8	M	63	Eradicated
IM9	F	80	Eradicated
IM10	M	40	Eradicated
IM11	M	67	Eradicated
IM12	F	84	Positive
IM13	F	85	Eradicated
IM14	F	66	Eradicated
IM15	M	75	Eradicated
IM16	M	75	Eradicated
IM17	M	64	Negative
IM18	F	82	Eradicated
IM19	F	52	Eradicated
IM20	M	86	Positive
IM21	F	64	Eradicated

Table 1. Continued

Sample ID	Sex	Age, y	<i>H pylori</i> status
IM22	M	76	Positive
IM23	F	54	Positive
IM24	F	33	Eradicated
IM25	M	61	Negative
IM26	M	86	Eradicated
IM27	M	68	Eradicated
Intestinal-type gastric cancer			
GCI1	F	80	Negative
GCI2	F	57	Positive
GCI3	M	71	Eradicated
GCI4	M	87	Eradicated
GCI5	F	78	Negative
GCI6	M	66	Negative
GCI7	M	53	Positive
GCI8	F	82	ND
GCI9	F	79	Positive
GCI10	M	72	Negative
GCI11	M	86	Negative
GCI12	F	79	Eradicated
GCI13	M	88	Negative
GCI14	F	77	Eradicated
GCI15	F	82	ND
GCI16	M	70	0
GCI17	M	70	Positive
GCI18	F	95	Positive
GCI19	M	88	Negative
GCI20	F	98	ND
GCI21	M	86	Negative
GCI22	M	62	ND
GCI23	F	58	ND
GCI24	M	86	Eradicated
GCI25	M	73	Eradicated
GCI26	F	80	Negative
GCI27	F	98	Positive
GCI28	M	82	ND
GCI29	F	95	Eradicated
GCI30	F	84	Eradicated
Diffuse-type gastric cancer			
GCd1	F	86	Negative
GCd2	F	77	Eradicated
GCd3	M	71	Eradicated
GCd4	F	75	Eradicated
GCd5	M	69	Negative
GCd6	M	77	Eradicated
GCd7	F	81	Negative
GCd8	F	82	Negative
GCd9	F	58	ND
GCd10	M	98	ND
GCd11	F	83	ND
GCd12	M	82	Negative
GCd13	F	94	ND
GCd14	M	89	Positive
GCd15	F	87	Eradicated
GCd16	F	86	Eradicated
GCd17	M	76	Positive
GCd18	M	34	Eradicated
GCd19	M	85	ND
GCd20	M	51	Positive
GCd21	M	72	Negative
GCd22	M	51	ND
GCd23	F	85	Negative
GCd24	F	91	Eradicated
GCd25	F	81	Negative
GCd26	F	78	Positive

ND, not determined.

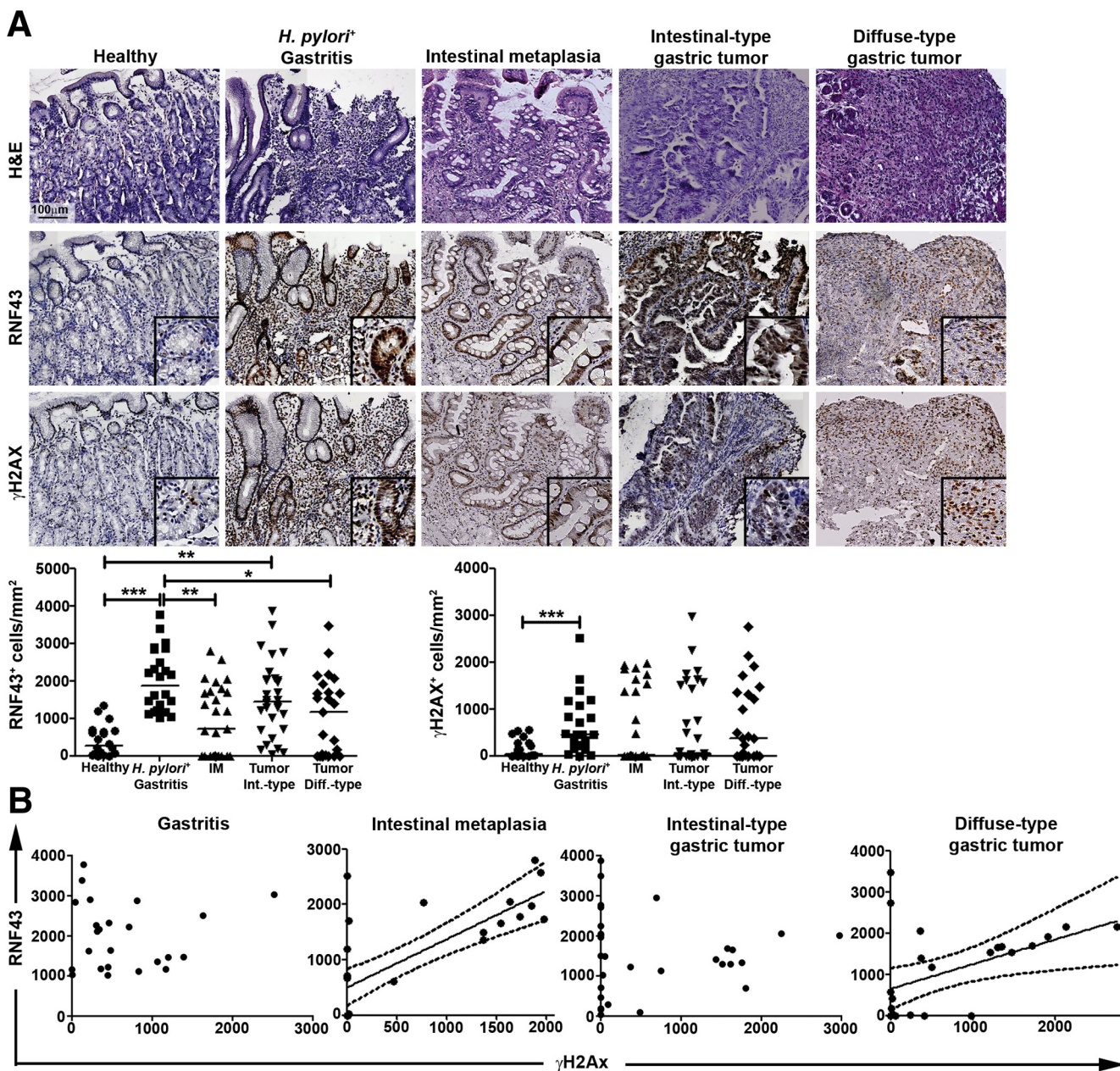


Figure 7. RNF43 expression varies during gastric carcinogenesis. (A) Representative images and quantification of RNF43 and γ H2AX-positive cells per square millimeter of human gastric tissue of healthy individuals ($n = 20$), and patients with gastritis ($n = 24$), intestinal metaplasia ($n = 27$), and intestinal-type ($n = 20$) or diffuse ($n = 25$) gastric cancer. Horizontal lines represent the median values. Each dot represents 1 sample. $*P \leq .05$, $**P \leq .01$, and $***P \leq .001$, 1-way analysis of variance multiple comparisons. (B) Spearman correlation between the number of RNF43 and γ H2AX-positive cells per square millimeter of human gastric tissue. Diff, diffuse; IM, intestinal metaplasia; Int, intestinal.

extensively as a central post-translational modification for the initiation^{19,34} and maintenance^{17,18,33} of DDR signaling.

The expression of RNF43 was found to be increased upon DNA damage. Top transcription factor binding sites described in the *RNF43* gene promoter include aryl hydrocarbon receptor (AhR), Activator protein 1 (AP-1), Aryl Hydrocarbon Receptor Nuclear Translocator (Arnt), c-Fos Proto-Oncogene, AP-1 Transcription Factor Subunit (c-Fos), c-Jun Proto-Oncogene, AP-1 Transcription Factor Subunit (c-Jun), Forkhead Box O4 (FOXO4), and Peroxisome

Proliferator Activated Receptor Gamma (PPAR- γ) (GeneCards). All of these transcription factors have been implicated in different aspects of the DDR, and therefore could be regulating RNF43 expression upon DNA damage. The identification of the transcription factors involved and the regulatory mechanisms behind it require further investigation.

H. pylori infection is the main risk factor for GC development. Previous studies have indicated that *H. pylori* can induce DNA damage directly to host cells through interaction of the type IV secretion system with integrin β 1. This

Table 2. List of Mutations Found in Human Gastric Tissue Samples

Sample	RNF43 SNPs	RNF43 mutations	Other mutations	MSI status
Intestinal metaplasia				
IM1	p.I47V p.R117H p.P686R	–	APC p.A1471Gfs*14 BRAF p.N581S	
IM2	p.I47V p.R117H	–	APC p.R1445fs KRAS p.G13D	
IM3	p.R117H p.P686R	–	–	
IM4	–	–	ERBB4 p.L713V	
IM5	p.I47V p.R117H	–	APC p.R1432X	
IM6	p.L418M p.R117H p.P686R	–	–	
IM7	p.R117H	–	–	
IM8	p.I47V p.L418M p.P686R	–	–	
IM9	p.R117H p.L418M	–	–	
IM10	p.I47V	–	–	
IM11	p.R117H	–	–	
IM12	p.I47V p.R117H p.L418M	–	–	
Intestinal-type gastric cancer				
Gci1	p.I47V p.R117H p.L418M	–	PTPRT p.P1075Rfs PIK3CA p.E542K TLR4 p.L10M	
Gci2	p.P686R	–	ERBB2 p.V842I	MSS
Gci3	p.R117H p.P760P	–	MDM2 amplification	
Gci4	–	–	Sox2 p.E36G APC p.R1432X PREX2 p.L50V TP53 p.G66R TP53 p.E204X	
Gci5	p.I47V p.R117H p.L418M	–	TP53 p.R116Q TP53 p.Y88H CDKN2A p.Q50H	
Gci6	p.I47V p.L418M p.P686R	–	TLR4 p.L298V PTPRT p.E911G	
Gci7	p.I47V p.R117H	–	ARID1A p.P1467fs PTEN M134T TP53 R151H	
Gci8	p.I47V p.L418M p.P686R	–	–	
Gci9	WT	–	–	
Gci10	p.I47V p.L418M	–	–	MSS
Gci11	p.I47V p.R343H p.L418M	–	CDKN2A p.Q70X PTEN p.R130X TGFB2 p.D405N	
Gci12	R117H	–	–	MSS
Gci13	p.I47V	–	TP53 p.G134E	
Gci14	p.L418M p.I47V p.R117H	p.R371R p.D628G p.R132X	APC p.R1432X CCND1 p.S257P	MSS
Gci15	–	–	FBXW7 p.A508D RHOA p.Y42C ARID1A p.P2095fs	MSI

Table 2. Continued

Sample	RNF43 SNPs	RNF43 mutations	Other mutations	MSI status
Diffuse-type gastric cancer				
GCd1	p.I47V	–	PREX2 p.R186Q	
GCd2	p.L418M	–	–	
	p.I47V			
GCd3	p.R117H	p.R584fs	ERBB2 p.R678Q CDH1 p.E429G	MSS
	p.P686R			
GCd4	–	–	–	MSS
GCd5	p.I47V	–	CDH1 p.D254H	
	p.L418M			
GCd6	–	–	–	
GCd7	p.L418M	p.R132X	TP53 p.R117M ARID1A p.R2158L	MSS
	–			
GCd8	p.I47V	–	CDH1 c.531+1G>T	MSS
GCd9	p.R343H	–	CDH1 p.E243K	MSS
	p.L418M			
GCd10	p.I47V	–	KRAS p.G13D TP53 p.R150W PIK3CA p.N345K PIK3CA p.A1066V MTOR p.R2317I	
	p.L418M			
GCd11	p.P686R	–	–	
GCd12	p.I47V	–	–	
GCd13	p.L418M	–	PIK3CA p.H1047R	
	p.I47V			
	p.L418M			

MSS, microsatellite stable.

interaction would lead to the activation of nuclear factor- κ B signaling and thereby to the activation of nucleotide excision repair endonucleases responsible for inducing DSBs.²⁶ In contrast, the involvement of other virulence factors such as vacuolating cytotoxin A (VacA) in the induction of DSBs was excluded.²⁵ Whether these virulence factors play a role in the RNF43-mediated DDR therefore deserves further investigations.

Current treatment of GC patients includes adjuvant chemotherapy with cisplatin or 5-fluorouracil, as well as irradiation.³⁵ The efficacy of these treatments to eliminate tumor cells is based on their ability to induce DNA damage. However, not all tumors respond to adjuvant therapy, and biomarkers that could predict response still are lacking. In a previous study, overexpression of RNF43 was shown to render gastric cells more susceptible to oxaliplatin and 5-fluorouracil, but the molecular mechanisms involved remained unclear.³⁶ In line with this observation, we also found that loss of RNF43 function confers resistance to DNA damage-inducing chemotherapy. More importantly, we identified the mechanism responsible, namely the direct role of RNF43 in DDR.³⁶

Furthermore, we observed a correlation between response to chemotherapy and RNF43 expression levels in human gastric organoids, indicating that not only loss of functional protein but also its down-regulation or up-regulation might modify resistance to DNA damage-inducing chemotherapeutics. We postulate that treating

patients expressing low levels of RNF43, or carrying mutations affecting its functional domain, with DNA-damaging drugs and radiation therapy (as recommended in the guidelines²⁸) would lead to detrimental effects. Thus, cells lacking RNF43 not only would resist radiotherapy or chemotherapy-induced apoptosis, but eventually would accumulate additional mutations induced by the treatments themselves, contributing to tumor progression and thereby worsening prognosis. Along these lines, decreased RNF43 expression has been associated with distant metastasis, TNM stage, and poorer overall survival of GC patients,³⁶ supporting our hypothesis. It also is relevant to note that *RNF43* mutations are highly enriched in MSI gastric tumors,^{8,11,12,30} which are characterized by a high mutation burden in tandem repeats³⁷ caused by deficient DNA repair machinery.³⁸ Therefore, it is plausible that acquired mutations in *RNF43* may contribute to the increased mutation rate in MSI tumors by further impairing DDR activation.

Our data suggest that mutations downstream of the catalytic domain of RNF43 still would retain functionality. This observation is in line with recent data showing that, for instance, the most common RNF43 mutation in gastric tumors (G659Vfs*41) is still fully functional in terms of WNT inhibition.³⁹

In light of our findings, the inclusion of *RNF43* in GC gene panels for the screening of patients should be considered to select therapeutic regimens based on mutation status. This,

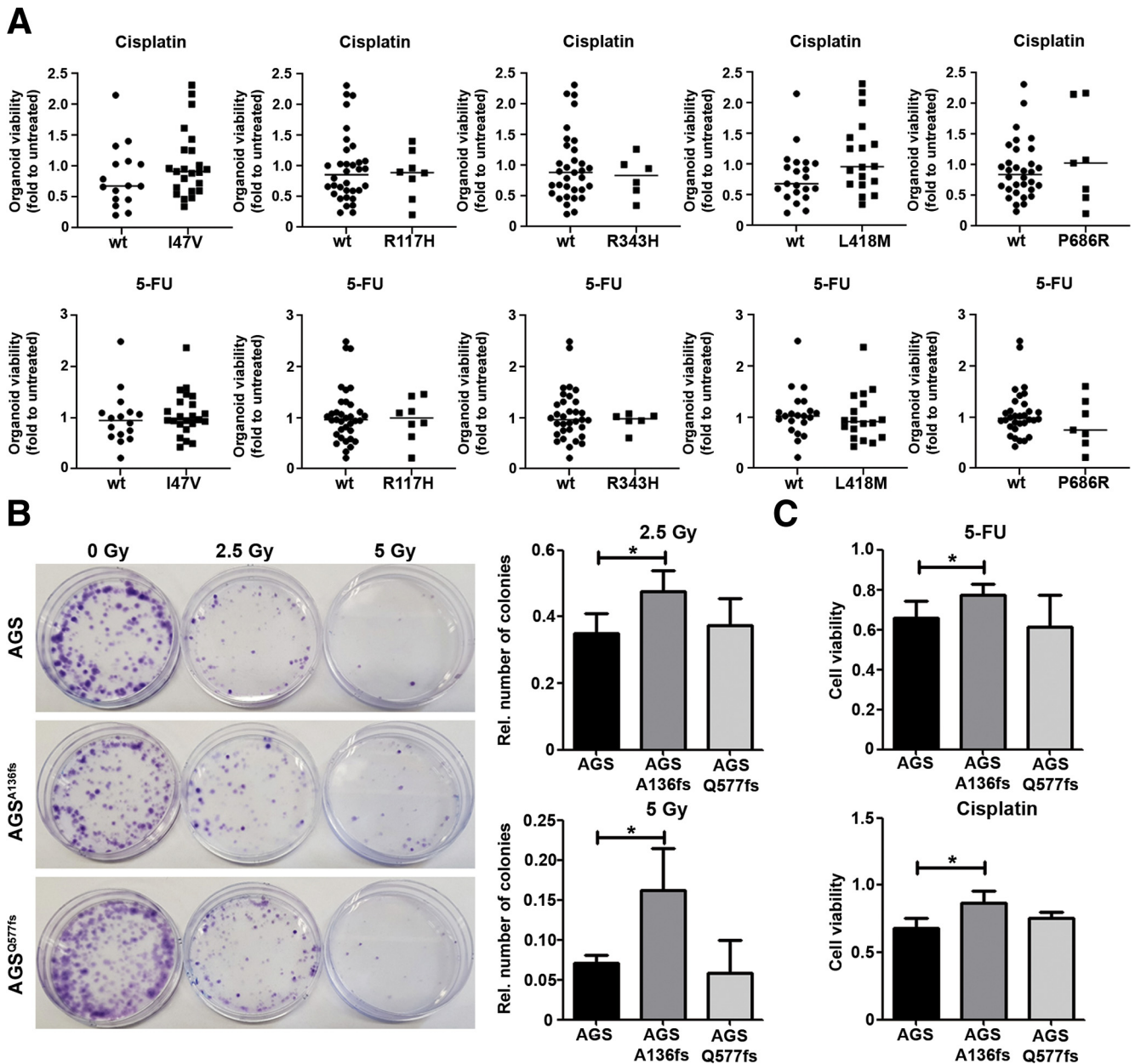


Figure 8. RNF43 mutations upstream of the RING domain confer resistance to DNA damage. (A) Viability of gastric organoids ($n = 40$) carrying different SNP variants of *RNF43* after treatment with 5-fluorouracil (5-FU) or cisplatin. Fold change was calculated over untreated organoids. Horizontal lines represent the median values. Mann–Whitney test. (B) Representative images and quantification of cell colonies after γ -radiation. ($n = 4$). (C) Cell viability after treatment with 5-FU or cisplatin. Values were normalized over untreated cells ($n = 4$). Error bars indicate SD. * $P \leq .05$, 2-tailed unpaired t test. Rel, relative.

together with the examination of protein expression levels of WT RNF43, may serve as a biomarker for therapy selection for GC patients. Moreover, screening of *RNF43* mutations and expression also could be considered for other types of tumors such as colorectal or pancreatic cancers, where mutations in *RNF43* have been observed frequently. In fact, and as mentioned earlier, a possible role of RNF43 in DDR in pancreatic cells already has been suggested.⁴⁰ As such, further investigations in other tissues will be important to confirm a general function of RNF43 as a modulator of DDR.

Materials and Methods

Cell Culture and Cell Treatments

AGS (ATCC CRL-1739) and MKN45 (RCB1001) cells were cultured in Dulbecco's modified Eagle medium (Invitrogen, Carlsbad, CA) containing 10% fetal calf serum (Sigma-Aldrich, St. Louis, MO) at 37°C in a humidified atmosphere (5% CO₂). Cells were tested routinely for *Mycoplasma* contamination. Short tandem repeat analysis was performed for authentication of the cell lines used. AGS and MKN45 shControl and shRNF43 cells were generated using

lentiviruses as previously described.¹³ Sequences are listed in Table 3.

AGS^{D196fs}, AGS^{A136fs}, and AGS^{Q577fs} cells were generated by CRISPR/Cas9. To generate AGS^{D196fs} cells, we

used guide RNAs targeting exon 6 of *RNF43* to introduce a 4-bp deletion at aspartic acid 196. The resulting frameshift mutation leads to a premature stop codon 5 amino acids downstream, deleting the functional RING

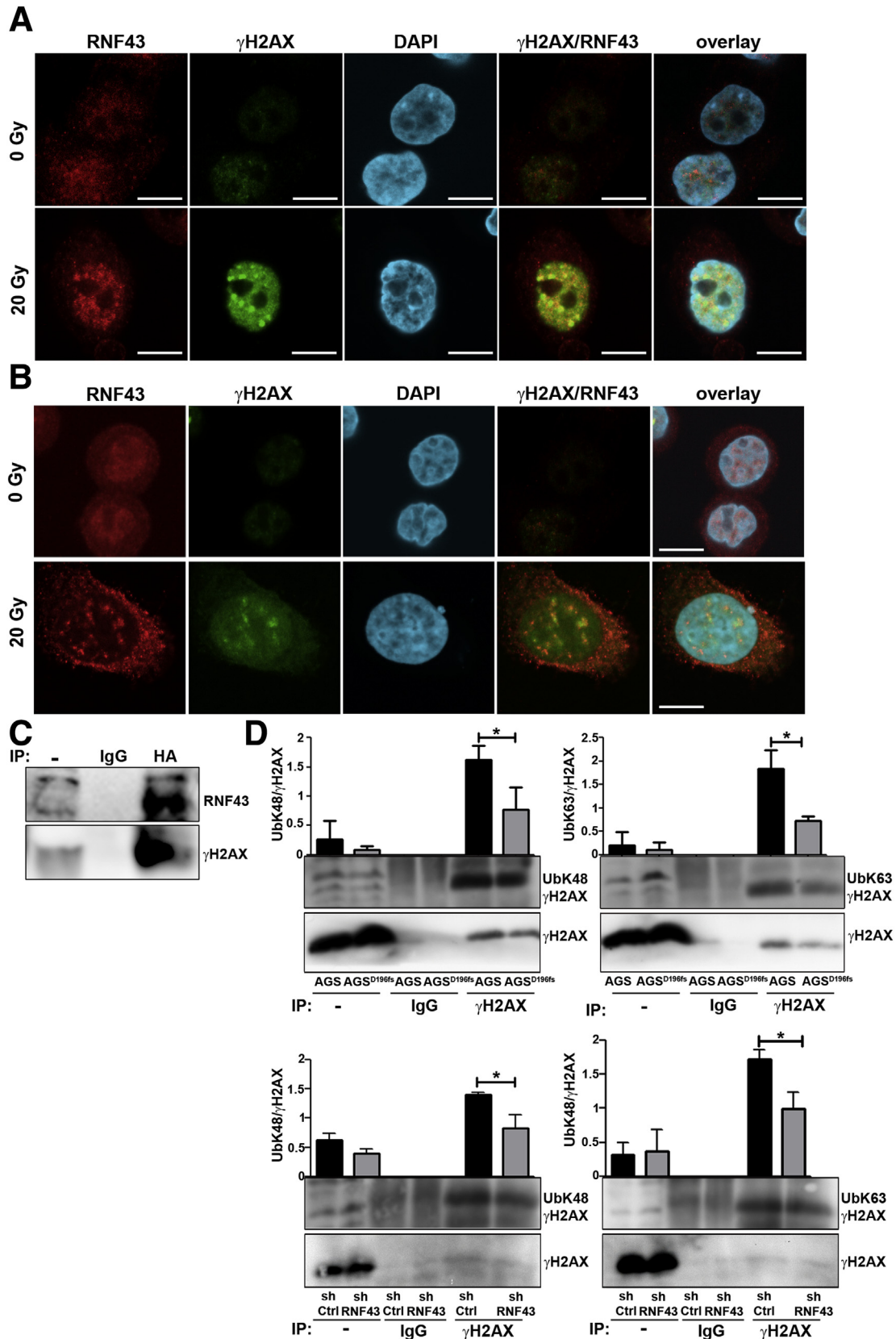


Table 3. DNA-Oligo Sequences for Lentiviral Knockdown and CRISPR/Cas9 Editing

Oligo	Forward	Reverse
shRNF43 1	GGAGAAAGCTATTGCACAGAA	TTCTGTGCAATAGCTTTCTCC
shRNF43 2	CGCGTCCCCTTCTTGGTAAGATC GAGAGTTCAAGAGACTCTCGATCTT ACCAAGAATTTTTGGAAAT	CGATTTCAAAAATTCTTGGTAAGAT CGAGAGTCTTTGAACTCTCGATCT TACCAAGAA GGGGA
shctrl 1	GCAACTTCAGCTATATCATT	AAATGATATAGCTGAAGTTGC
shctrl 2	CGCGTCCCCGTACAGCCGCTCAATTCT TTCAAGAGAAGAATTGAGGCGGCTGT ACTTTTTGGAAAT	CGATTTCAAAAAGTACAGCCGCTCA ATTCTTCTTTGAAAGAATTGAGGCGGCT GTACGGGGA
Guide RNA CRISPR/Cas9 AGS ^{D196fs}	CCACACATCATAATCTGGCT	AGCCAGATTATGATGTGTGG
Guide RNA CRISPR/Cas9 AGS ^{R132X}	GATGTCAAAGAGGACAGCAC	-
Guide RNA CRISPR/Cas9 AGS ^{R584fs}	AAACCGGAGTCCCCAGTCC	-

domain. Guide RNA sequences (Table 3) were designed using www.tools.genome-engineering.org, annealed, and cloned into a pX330 vector (42230; Addgene, Watertown, Massachusetts, USA) containing green fluorescent protein (GFP). Cells were transfected with Lipofectamine 2000 (Invitrogen), sorted for GFP, and grown as single-cell colonies. Genomic DNA was extracted using the Pure-Link Genomic DNA Mini Kit (Invitrogen), and mutations in *RNF43* and selected off targets were checked by Sanger sequencing.

For targeted mutations, Cas9 ribonucleoproteins (RNPs) were transfected together with an oligonucleotide containing the desired mutations and homology arms flanking 30 bp of the site of interest on both sides. Guide RNA and repair oligonucleotides were planned using Benchling (www.benchling.com), and guide RNAs, ATTO 550-labeled tracer RNA, and Cas9 protein were purchased from Integrated DNA Technologies (Coralville, IA). Repair oligonucleotides were purchased as single-stranded DNA, as follows:

R132X: TGCCTCTGCAGGCTCGGATGGCGGGTGAGTG
AGGAGCAAGTGCTGTCTCTTTGACATCA;

R584fs: CAGAAACCGGAGTCCCCAGTCCAGAC
CTCCTATTCTCTCGACAGCCCCAGCCAGCCACCTTCTCCT.

RNP assembly and transfection were performed as described by Integrated DNA Technologies. AGS cells (5×10^5) were electroporated with RNPs using a Nucleofector 4D (Kit X, pulse code DS-135; Lonza, Basel, Switzerland). To increase homology-directed repair, Nu7026 (20 $\mu\text{mol/L}$; Sigma-Aldrich) and Trichostatin A (0.01 $\mu\text{mol/L}$; Sigma-Aldrich) were added. At 24 hours after electroporation, cells were sorted for ATTO 550 and seeded as single-cell clones for selection.

Lipofectamine 2000 (Invitrogen) was used for plasmid transfections. Transfected cells were cultured for 36 hours

before being subjected to γ -radiation and subsequent co-immunoprecipitation.

γ -radiation was performed using a Cs¹³⁷ radiation source (Buchler, Braunschweig, Germany). For chemotherapeutic treatment, cells were seeded in a 96-well plate (7500 cells/well) and treated with 5-fluorouracil (2 $\mu\text{g/mL}$) or cisplatin (10 $\mu\text{g/mL}$) for 48 hours, followed by measurement of cell viability using Cell-counting kit 8 (Sigma-Aldrich).

Cell Viability and Clonogenicity Assay

AGS and MKN45 cells were seeded in a 96-well plate (2500 cells/well) after γ -radiation, and serum-starved for 24 hours. After addition of serum-containing medium, cells were allowed to grow for 48 hours and cell viability was measured using Cell-counting kit 8 (Sigma-Aldrich).

To assess clonal expansion, AGS and MKN45 cells were irradiated and seeded at low density. After 14 days, single-cell colonies were fixed and stained with 6% glutaraldehyde containing Crystal Violet.

Annexin V Staining

Four days (AGS) or 6 days (MKN45) after γ -radiation, cells were stained with Annexin V Pacific Blue conjugate (Invitrogen) and propidium iodide (Sigma-Aldrich). Fluorescence was measured in a CyAn ADP flow cytometer (Beckman Coulter, Brea, CA) and analyzed with FlowJo (Becton, Dickinson & Company, Franklin Lakes, NJ).

H. pylori Infection

H. pylori strain PMSS1⁴¹ was cultured on Wilkins-Chalgren Dent agar plates in a microaerophilic atmosphere.

Figure 9. (See previous page). **RNF43 is up-regulated in response to DNA damage and it is recruited to sites of DNA damage.** Representative immunofluorescence images of RNF43 (red) and γ H2AX (green) in control and irradiated (A) AGS and (B) MKN45 cells. Scale bars: 10 μm . (C) Immunoprecipitation of RNF43 (human influenza hemagglutinin, HA) from AGS cells transfected with HA-tagged RNF43 upon γ -radiation (20 Grey), followed by Western blot analysis ($n = 3$; 1 representative experiment is shown). (D) Immunoprecipitation of γ H2AX from AGS and MKN45 cells after radiation (20 Grey), followed by Western blot analysis. -, whole lysate. Quantification of ubiquitinated γ H2AX from total γ H2AX is shown ($n = 3$). Error bars indicate SD. * $P \leq .05$, 2-tailed unpaired t test. DAPI, 4',6-diamidino-2-phenylindole; IP, immunoprecipitation.

Table 4. Sequences of the Primers Used in This Study

Primer	Human		Murine	
	Forward	Reverse	Forward	Reverse
GAPDH	GAAGGTGAAGGTCGGAGT	GAAGATGGTGATGGGATTTTC	GCCTTCTCCATGGTGGTGAA	GCACAGTCAAGGCCGAGAAT
RNF43 (qPCR)	GAGTGTGCTCCAGATGTGT	AGTCCTCTTCCA GTCCTTCTA	GGGGCAAACATATGACCGTGTG	CTGCTGAAGAGGATCCGGTC
AXIN2	CTC CCC ACC TTG AAT GAA GA	GTT TCC GTG GAC CTC ACA CT		
LGR5	TGA TGA CCA TTG CCT ACA C	GTA AGG TTT ATT AAA GAG GAG AAG		
<i>lfrng</i>	-	-	TCAAGTGGCATAGATGTGGAAGAA	TGGCTCTGCAGGATTTTCATG
<i>Cxcl1</i>	-	-	TGCACCCAAACCCGAAGTCAT	TTGTCAGAAGCCAGCGTTTCAC
<i>TNFα</i>	-	-	CGATGGTTGTACCTTGTC	CGGACTCCGCAAAGTCTAAG

Cells were infected at a multiplicity of infection (MOI) of 50 and 100 ($OD_{600} 1 = 2 \times 10^8$ bacteria/mL) for 24 hours, and lysed in sodium dodecyl sulfate (SDS) sample buffer or RNA lysis buffer.

Quantitative Polymerase Chain Reaction

GenElute Mammalian Total RNA Miniprep Kit (Sigma-Aldrich) was used to isolate RNA. Mouse tissue was homogenized using a Precellys (Bertin Instruments, Montigny-le-Bretonneux, France) lysing kit. MMLV Reverse Transcriptase RNase H–Point Mutant (Promega, Madison, WI) was used for reverse transcription. Transcript abundance was assessed using the GoTaq quantitative polymerase chain reaction Mastermix (Promega) and a CFX384 system (Bio-Rad, Hercules, CA). Primer sequences are included in Table 4. Gene expression was analyzed with the comparative relative expression ($\Delta\Delta C_T$) method.

Immunofluorescence

Cells were seeded on glass coverslips either untreated or immediately after being subjected to γ -radiation (20 Gy). Immunofluorescence staining was performed as previously described.¹³ The monoclonal antibody GGTRNF 8D6 (IgG2b/k) was raised in rats against amino acid residues 329–348 (SRSYQEPGRRLHLIRQHPGH) of human RNF43. Staining was analyzed using a FluoView FV10i confocal microscope (Olympus, Shinjuku, Japan).

Co-immunoprecipitation and Western blot

Cells were lysed in RIPA buffer (50 mmol/L Tris-HCl, pH 7.4, 1% Nonidet P-40 (NP-40), 150 mmol/L NaCl, 0.25% Deoxycholate (DOC), 1 mmol/L ethylene glycol-bis(β -aminoethyl ether)-*N,N,N,N*-tetraacetic acid) containing phosphatase and protease inhibitors and precleared using 1 μ g appropriate IgG and agarose conjugate. Lysates were centrifuged at 3000 rpm for 1 minute at 4°C, and incubated with primary antibody or IgG overnight at 4°C while rotating. Protein A/G agarose beads (Roche, Basel, Switzerland) were added to the lysates and incubated for 4 hours at 4°C. After washing with phosphate-buffered saline, beads were collected by centrifugation, diluted in SDS sample buffer for Western blot, and boiled for 5 minutes at 95°C.

Protein lysates were subjected to SDS–polyacrylamide gel electrophoresis and transferred to a nitrocellulose membrane. After blocking with 5% low-fat milk in Tris-buffered saline-tween (TBS-T), membranes were incubated in primary antibody (Table 5) overnight at 4°C. Membranes were washed in TBS-T followed by incubation with horseradish peroxidase–conjugated secondary antibodies for 1 hour at room temperature. Signal was visualized using Clarity ECL Western substrate (Bio-Rad) and an Intas chemiluminescence detection system (Intas, Göttingen, Germany).

Gastric Organoids

Gastric organoid culture was established as previously described.⁴² There were 100 (48-well plate) or 300 (24-well plate) gastric glands seeded per well.

Table 5.Antibodies Used in This Study

Target	Clone	Assay	Dilution	Company	Reactivity
Annexin V, Pacific Blue conjugate		Flow cytometry	1:100	Thermo Fisher	H, M
(non-p-) β -catenin	D2U8Y	IHC	1:1000	Cell Signaling (Danvers, MA)	H, M
CD3	SP7	IHC	1:150	Thermo Fisher	H, M
Chk2	1C12	WB	1:1000	Cell Signaling	H
Cleaved caspase 3 (Asp175)	9661	IHC	1:300	Cell Signaling	H, M
GAPDH	14C10	WB	1:1000	Cell Signaling	H, M
HA	H6908	IP	1:100	Sigma	–
HA	H3663	WB	1:1000	Sigma	–
Ki67	D2H10	IHC	1:400	Cell Signaling	H
p-Chk2 (Thr68)	C13C1	WB	1:1000	Cell Signaling	H
RNF43	HPA008079	IHC	1:1000	Invitrogen (ATLAS)	H
RNF43	8D6	IF	1:150	–	H
K48-linked Ubiquitin	D9D5	WB	1:1000	Cell Signaling	H
K63-linked Ubiquitin	D7A11	WB	1:1000	Cell Signaling	H
γ H2Ax	ab81299	WB, IHC, IF	1:10000 (WB) 1:5000 (IHC) 1:300 (IF)	Abcam	H, M
γ H2Ax	5438	IP	1:50	Cell Signaling	H, M

GAPDH, glyceraldehyde-3-phosphate dehydrogenase; H, human; IF, immunofluorescence; IHC, immunohistochemistry; IP, immunoprecipitation; M, mouse; WB, Western blot.

After 1 week, organoids were incubated with 5-fluorouracil (2 $\mu\text{g}/\text{mL}$) or cisplatin (10 $\mu\text{g}/\text{mL}$) for 4 (murine) or 5 (human) days. Viability was analyzed using Cell Titer Glo 3D (Promega). Luminescence was measured using a SpectraMax plate reader (Molecular Devices, San José, CA). Viability was normalized to untreated controls. For human organoids, an organoid viability normalized to control greater than 95% was defined as a nonresponder, while organoids with a viability of less than 95% were defined as responders.

Animal Experiments

Friend Virus B NIH Jackson (FVBN) WT and *Rnf43*^{ΔEx8} mice¹³ were used for in vivo experiments. *Rnf43*^{ΔEx8} mice were generated by introducing a 57-bp deletion in exon 8 of the genomic sequence of *Rnf43* using CRISPR/Cas9 technology. This deletion led to a systemic loss of the functional RING domain of Rnf43. Mice were co-housed under specific pathogen-free conditions in individually ventilated cages (Tecniplast, Hohenpeißenberg, Germany) containing enrichment material. Mice were fed a rodent diet (Envigo, Indianapolis, IN) ad libitum.

Eight- to 10-week-old male and female FVBN WT or *Rnf43*^{ΔEx8} mice were infected twice with 2×10^8 *H pylori* PMSS1 diluted in 200 μL Brain heart infusion (BHI) 20% fetal calf serum by oral gavage. Mice were killed after 3 months.

Xenograft tumors were established as previously described.¹³ Tumor volume was measured with a caliper and calculated as follows: volume = length*width*height/2. When tumors reached a volume of 40–70 mm³, mice were injected with 20 mg/kg 5-fluorouracil or 10 mg/kg cisplatin twice a week. When tumors reached a size of 500 mm³, mice were killed and tumors were resected.

Immunohistochemistry

Mouse gastric samples were fixed in 4% formaldehyde and embedded in paraffin. Heat-induced antigen retrieval was performed using 10 mmol/L sodium citrate (pH 6). Primary antibodies were applied overnight (Table 5), and bound secondary antibodies were detected with diaminobenzidine. Slides were scanned and analyzed using an Olympus Virtual Slide Imaging System.

Sequencing

H&E-stained sections of gastric biopsy specimens were used to select the lesion to be analyzed. Sections (10- μm) were used to extract DNA with a GeneRead DNA FFPE Kit (Qiagen, Hilden, Germany). DNA concentrations were determined by a QuiBit 2.0 fluorometer (ThermoFisher, Waltham, MA) and the amplifiable genomic DNA was quantified using TaqMan RNase P detection kit (ThermoFisher). Barcoded libraries were generated using the Ion Xpress Barcode Adapters (ThermoFisher). Samples were purified using the Agencourt AMPure XP kit (Beckman Coulter) and quantified with the Ion Library TaqMan quantitation kit (ThermoFisher). Libraries were loaded on the Ion 530 chip kit

(ThermoFisher) and sequenced using an Ion S5XL sequencer (ThermoFisher).

Statistics

Data were first tested for normality using the Shapiro–Wilk test. Normally distributed data then were analyzed by the Student *t* test. The Mann–Whitney *U* test or the Kruskal–Wallis test for multiple comparisons was used to compare not normally distributed data. Results of at least 3 independent experiments were analyzed. Statistical significance was defined when $P < .05$.

Study Approval

Experiments with human gastric organoids were approved by the Ethics Committee of Klinikum Rechts der Isar (116/17 S).

All animal experiments were conducted in compliance with European guidelines for the care and use of laboratory animals and were approved by the Regierung von Oberbayern (AZ 55.2-1-55-2532-239-15 and AZ 55.2-1-54-2532-196-2016).

Formalin-fixed, paraffin-embedded human gastric samples (Table 1) were obtained from the tissue bank of the Institut für Pathologie at Klinikum Bayreuth (Germany) after approval of the local ethics committee (Project number 243_19Bc).

All authors had access to the study data and reviewed and approved the final manuscript.

References

1. Lauren P. Histogenesis of intestinal and diffuse types of gastric carcinoma. *Scand J Gastroenterol Suppl* 1991;180:160–164.
2. Correa P. Human gastric carcinogenesis: a multistep and multifactorial process—First American Cancer Society Award Lecture on Cancer Epidemiology and Prevention. *Cancer Res* 1992;52:6735–6740.
3. Cancer Genome Atlas Research Network. Comprehensive molecular characterization of gastric adenocarcinoma. *Nature* 2014;513:202–209.
4. Orditura M, Galizia G, Sforza V, Gambardella V, Fazio A, Laterza MM, Andreozzi F, Ventriglia J, Savastano B, Mabilia A, Lieto E, Ciardiello F, De Vita F. Treatment of gastric cancer. *World J Gastroenterol* 2014;20:1635–1649.
5. Aichler M, Lubber B, Lordick F, Walch A. Proteomic and metabolic prediction of response to therapy in gastric cancer. *World J Gastroenterol* 2014;20:13648–13657.
6. Kim ST, Cristescu R, Bass AJ, Kim KM, Odegaard JI, Kim K, Liu XQ, Sher X, Jung H, Lee M, Lee S, Park SH, Park JO, Park YS, Lim HY, Lee H, Choi M, Talasz A, Kang PS, Cheng J, Loboda A, Lee J, Kang WK. Comprehensive molecular characterization of clinical responses to PD-1 inhibition in metastatic gastric cancer. *Nat Med* 2018;24:1449–1458.

7. Lianos GD, Glantzounis GK, Bali CD, Katsios C, Roukos DH. Identification of novel genes by whole-exome sequencing can improve gastric cancer precision oncology. *Future Oncol* 2017;13:883–892.
8. Wang K, Yuen ST, Xu J, Lee SP, Yan HH, Shi ST, Siu HC, Deng S, Chu KM, Law S, Chan KH, Chan AS, Tsui WY, Ho SL, Chan AK, Man JL, Foglizzo V, Ng MK, Chan AS, Ching YP, Cheng GH, Xie T, Fernandez J, Li VS, Clevers H, Rejto PA, Mao M, Leung SY. Whole-genome sequencing and comprehensive molecular profiling identify new driver mutations in gastric cancer. *Nat Genet* 2014;46:573–582.
9. Maruvka YE, Mouw KW, Karlic R, Parasuraman P, Kamburov A, Polak P, Haradhvala NJ, Hess JM, Rheinbay E, Brody Y, Koren A, Braunstein LZ, D'Andrea A, Lawrence MS, Bass A, Bernards A, Michor F, Getz G. Analysis of somatic microsatellite indels identifies driver events in human tumors. *Nat Biotechnol* 2017;35:951–959.
10. Cho J, Ahn S, Son DS, Kim NK, Lee KW, Kim S, Lee J, Park SH, Park JO, Kang WK, An JY, Choi MG, Lee JH, Sohn TS, Bae JM, Kim S, Kim KM. Bridging genomics and phenomics of gastric carcinoma. *Int J Cancer* 2019;145:2407–2417.
11. Cho J, Chang YH, Heo YJ, Kim S, Kim NK, Park JO, Kang WK, Lee J, Kim KM. Four distinct immune microenvironment subtypes in gastric adenocarcinoma with special reference to microsatellite instability. *ESMO Open* 2018;3:e000326.
12. Jung SH, Kim SY, An CH, Lee SH, Jung ES, Park HC, Kim MS, Chung YJ, Lee SH. Clonal structures of regionally synchronous gastric adenomas and carcinomas. *Clin Cancer Res* 2018;24:4715–4725.
13. Neumeyer V, Grandl M, Dietl A, Brutau-Abia A, Allgauer M, Kalali B, Zhang Y, Pan KF, Steiger K, Vieth M, Anton M, Mejias-Luque R, Gerhard M. Loss of endogenous RNF43 function enhances proliferation and tumour growth of intestinal and gastric cells. *Carcinogenesis* 2019;40:551–559.
14. Koo BK, Spit M, Jordens I, Low TY, Stange DE, van de Wetering M, van Es JH, Mohammed S, Heck AJ, Maurice MM, Clevers H. Tumour suppressor RNF43 is a stem-cell E3 ligase that induces endocytosis of Wnt receptors. *Nature* 2012;488:665–669.
15. Loregger A, Grandl M, Mejias-Luque R, Allgauer M, Degenhart K, Haselmann V, Oikonomou C, Hatzis P, Janssen KP, Nitsche U, Gradl D, van den Broek O, Destree O, Ulm K, Neumaier M, Kalali B, Jung A, Varela I, Schmid RM, Rad R, Busch DH, Gerhard M. The E3 ligase RNF43 inhibits Wnt signaling downstream of mutated beta-catenin by sequestering TCF4 to the nuclear membrane. *Sci Signal* 2015;8:ra90.
16. Bohgaki M, Bohgaki T, El Ghamrasni S, Srikumar T, Maire G, Panier S, Fradet-Turcotte A, Stewart GS, Raught B, Hakem A, Hakem R. RNF168 ubiquitylates 53BP1 and controls its response to DNA double-strand breaks. *Proc Natl Acad Sci U S A* 2013;110:20982–20987.
17. Doil C, Mailand N, Bekker-Jensen S, Menard P, Larsen DH, Pepperkok R, Ellenberg J, Panier S, Durocher D, Bartek J, Lukas J, Lukas C. RNF168 binds and amplifies ubiquitin conjugates on damaged chromosomes to allow accumulation of repair proteins. *Cell* 2009;136:435–446.
18. Mailand N, Bekker-Jensen S, Fastrup H, Melander F, Bartek J, Lukas C, Lukas J. RNF8 ubiquitylates histones at DNA double-strand breaks and promotes assembly of repair proteins. *Cell* 2007;131:887–900.
19. Pan MR, Peng G, Hung WC, Lin SY. Mono-ubiquitination of H2AX protein regulates DNA damage response signaling. *J Biol Chem* 2011;286:28599–28607.
20. Smith J, Tho LM, Xu N, Gillespie DA. The ATM-Chk2 and ATR-Chk1 pathways in DNA damage signaling and cancer. *Adv Cancer Res* 2010;108:73–112.
21. Menoyo A, Alazzouzi H, Espin E, Armengol M, Yamamoto H, Schwartz S Jr. Somatic mutations in the DNA damage-response genes ATR and CHK1 in sporadic stomach tumors with microsatellite instability. *Cancer Res* 2001;61:7727–7730.
22. Kim JW, Im SA, Kim MA, Cho HJ, Lee DW, Lee KH, Kim TY, Han SW, Oh DY, Lee HJ, Kim TY, Yang HK, Kim WH, Bang YJ. Ataxia-telangiectasia-mutated protein expression with microsatellite instability in gastric cancer as prognostic marker. *Int J Cancer* 2014;134:72–80.
23. Touati E, Michel V, Thiberge JM, Wuscher N, Huerre M, Labigne A. Chronic *Helicobacter pylori* infections induce gastric mutations in mice. *Gastroenterology* 2003;124:1408–1419.
24. Butcher LD, den Hartog G, Ernst PB, Crowe SE. Oxidative stress resulting from *Helicobacter pylori* infection contributes to gastric carcinogenesis. *Cell Mol Gastroenterol Hepatol* 2017;3:316–322.
25. Toller IM, Neelsen KJ, Steger M, Hartung ML, Hottiger MO, Stucki M, Kalali B, Gerhard M, Sartori AA, Lopes M, Muller A. Carcinogenic bacterial pathogen *Helicobacter pylori* triggers DNA double-strand breaks and a DNA damage response in its host cells. *Proc Natl Acad Sci U S A* 2011;108:14944–14949.
26. Hartung ML, Gruber DC, Koch KN, Gruter L, Rehauer H, Tegtmeyer N, Backert S, Muller AH. *pylori*-induced DNA strand breaks are introduced by nucleotide excision repair endonucleases and promote NF-kappaB target gene expression. *Cell Rep* 2015;13:70–79.
27. Santos JC, Gambeloni RZ, Roque AT, Oeck S, Ribeiro ML. Epigenetic mechanisms of ATM activation after *Helicobacter pylori* infection. *Am J Pathol* 2018;188:329–335.

28. Smyth EC, Verheij M, Allum W, Cunningham D, Cervantes A, Arnold D; ESMO Guidelines Committee. Gastric cancer: ESMO Clinical Practice Guidelines for diagnosis, treatment and follow-up. *Ann Oncol* 2016; 27(Suppl 5):v38–v49.
29. Wen D, Wang G, Huang Z, Cui X, Song J, Zhu Z, Cui L. Reduced frequency and prognostic significance of ring finger protein 43 nucleotide polymorphisms in a Chinese colorectal cancer cohort. *DNA Cell Biol* 2019; 38:541–548.
30. Min BH, Hwang J, Kim NK, Park G, Kang SY, Ahn S, Ahn S, Ha SY, Lee YK, Kushima R, Van Vrancken M, Kim MJ, Park C, Park HY, Chae J, Jang SS, Kim SJ, Kim YH, Kim JI, Kim KM. Dysregulated Wnt signalling and recurrent mutations of the tumour suppressor RNF43 in early gastric carcinogenesis. *J Pathol* 2016; 240:304–314.
31. Wang H, Wang L, Erdjument-Bromage H, Vidal M, Tempst P, Jones RS, Zhang Y. Role of histone H2A ubiquitination in Polycomb silencing. *Nature* 2004; 431:873–878.
32. Wang B, Elledge SJ. Ubc13/Rnf8 ubiquitin ligases control foci formation of the Rap80/Abraxas/Brca1/Brcc36 complex in response to DNA damage. *Proc Natl Acad Sci U S A* 2007; 104:20759–20763.
33. Mattioli F, Vissers JH, van Dijk WJ, Ikpa P, Citterio E, Vermeulen W, Marteijn JA, Sixma TK. RNF168 ubiquitinates K13–15 on H2A/H2AX to drive DNA damage signaling. *Cell* 2012;150:1182–1195.
34. Wu CY, Kang HY, Yang WL, Wu J, Jeong YS, Wang J, Chan CH, Lee SW, Zhang X, Lamothe B, Campos AD, Darnay BG, Lin HK. Critical role of monoubiquitination of histone H2AX protein in histone H2AX phosphorylation and DNA damage response. *J Biol Chem* 2011; 286:30806–30815.
35. Kim IH. Current status of adjuvant chemotherapy for gastric cancer. *World J Gastrointest Oncol* 2019; 11:679–685.
36. Gao Y, Cai A, Xi H, Li J, Xu W, Zhang Y, Zhang K, Cui J, Wu X, Wei B, Chen L. Ring finger protein 43 associates with gastric cancer progression and attenuates the stemness of gastric cancer stem-like cells via the Wnt-beta/catenin signaling pathway. *Stem Cell Res Ther* 2017;8:98.
37. Yamamoto H, Imai K. Microsatellite instability: an update. *Arch Toxicol* 2015;89:899–921.
38. Jackson SP, Bartek J. The DNA-damage response in human biology and disease. *Nature* 2009; 461:1071–1078.
39. Tu J, Park S, Yu W, Zhang S, Wu L, Carmon K, Liu QJ. The most common RNF43 mutant G659Vfs*41 is fully functional in inhibiting Wnt signaling and unlikely to play a role in tumorigenesis. *Sci Rep* 2019; 9:18557.
40. Gala MK, Mizukami Y, Le LP, Moriichi K, Austin T, Yamamoto M, Lauwers GY, Bardeesy N, Chung DC. Germline mutations in oncogene-induced senescence pathways are associated with multiple sessile serrated adenomas. *Gastroenterology* 2014;146:520–529.
41. Arnold IC, Lee JY, Amieva MR, Roers A, Flavell RA, Sparwasser T, Muller A. Tolerance rather than immunity protects from *Helicobacter pylori*-induced gastric preneoplasia. *Gastroenterology* 2011;140:199–209.
42. Bartfeld S, Clevers H. Organoids as model for infectious diseases: culture of human and murine stomach organoids and microinjection of *Helicobacter pylori*. *J Vis Exp* 2015;105:53359.

Received June 25, 2020. Accepted November 6, 2020.

Correspondence

Address correspondence to: Raquel Mejias-Luque, PD, PhD, Trogerstrasse 30, Munich 81675, Germany. e-mail: raquel.mejias-luque@tum.de; fax: (49) 089-4140-4139.

Acknowledgments

The authors thank Martina Grandl, Karin Mink, Raphaela P. Semper, Andreas Wanisch, and Nicolai Buse for their invaluable technical assistance, and Claudia Crowell for proofreading the manuscript.

CRedit Authorship Contributions

Victoria Neumeyer (Formal analysis: Lead; Investigation: Lead; Methodology: Lead; Writing: Lead; Formal analysis: Lead)
 Anna Brutau-Abia (Investigation: Supporting)
 Michael Allgäuer (Investigation: Supporting)
 Nicole Pfarr (Formal analysis: Supporting; Methodology: Supporting)
 Wilko Weichert (Resources: Supporting)
 Christina Falkeis-Veits (Formal analysis: Supporting)
 Elisabeth Kremmer (Methodology: Supporting)
 Michael Vieth (Formal analysis: Supporting)
 Markus Gerhard (Supervision: Supporting)
 Raquel Mejias Luque (Conceptualization: Lead; Formal analysis: Lead; Supervision: Lead; Writing: Lead)

Conflicts of interest

The authors disclose no conflicts.

Funding

Supported by Deutsche Forschungsgemeinschaft grant GE2042 12-1.